Engineering a novel probiotic toolkit in *Escherichia coli Nissle1917* for sensing and mitigating gut inflammatory diseases

Authors

Nathalie Weibel[1, †], Martina Curcio[1, †], Atilla Schreiber[1, †], Gabriel Arriaga[1 †], Marine Mausy[1 †], Jana Mehdy[1], Lea Brüllmann[1], Andreas Meyer[1], Len Roth[1], Tamara Flury[1], Valerie Pecina[1], Kim Starlinger[1], Jan Dernič[2], Kenny Jungfer[3], Fabian Ackle[4], Jennifer Earp[4], Martin Hausmann[5], Martin Jinek[3], Gerhard Rogler[5], Cauã Antunes Westmann[6,7*]

Affiliations

[1] – University of Zürich, Campus Irchel, Winterthurerstrasse 190, 8057 Zürich

[2] – Institute of Pharmacology and Toxicology, University of Zürich, Winterthurerstrasse 190, CH-8057 Zürich, Switzerland

[3] – Department of Biochemistry, University of Zürich, Winterthurerstrasse 190, CH-8057, Zürich, Switzerland

[4] – Institute of Medical Microbiology, University of Zürich, Gloriastrasse 28/30, CH-8006 Zürich, Switzerland

[5] - Department of Gastroenterology and Hepatology, University Hospital Zürich and Zürich University, Rämistrasse 100, 8091, Zurich, Switzerland

[6] – Department of Evolutionary Biology and Environmental Studies, University of Zürich, Winterthurerstrasse 190, Zürich CH-8057, Switzerland

[7] – Swiss Institute of Bioinformatics, Quartier Sorge-Batiment Genopode, 1015 Lausanne, Switzerland

† - Equal contribution

* - Corresponding author caua.westmann@ieu.uzh.ch

Significance

Probiotics can be engineered to detect and act upon extracellular disease indicators, optimizing therapeutic outcomes. Particularly, self-regulating sense-and-respond genetic circuits have the potential to enhance the accuracy, efficacy, and adaptability of treatment interventions. In this study, we developed and characterized a new integrated and modular toolkit that detects a gut inflammation biomarker, specifically nitric oxide, and responds to it in an inducible manner by secreting humanized nanobodies targeting the pro-inflammatory molecule TNFα. We also develop a coarse-grained mathematical framework for modelling engineered probiotic activity in the gut. This novel system contributes to current efforts to develop new engineered probiotic systems and holds promise for inspiring new treatments for gut inflammation associated with various autoimmune diseases.

Abstract

Inflammatory Bowel Disease (IBD) is characterized by chronic intestinal inflammation with no cure and limited treatment options that often have systemic side effects. In this study, we developed a target-specific system to potentially treat IBD by engineering the probiotic bacterium *Escherichia coli Nissle 1917* (EcN). Our modular system comprises three components: a transcription factor-based sensor (NorR) capable of detecting the inflammation biomarker nitric oxide, a type 1 hemolysin secretion system, and a therapeutic cargo consisting of a library of humanized anti-TNFα nanobodies. Despite a reduction in sensitivity, our system demonstrated a concentration-dependent response to nitric oxide, successfully secreting functional nanobodies with binding affinities comparable to the commonly used drug Adalimumab, as confirmed by ELISA and in vitro assays. This newly validated nanobody library expands EcN therapeutic capabilities. The adopted secretion system, also characterized for the first time in EcN, can be further adapted as a platform for screening and purifying proteins of interest. Additionally, we provided a mathematical framework to assess critical parameters in engineering probiotic systems, including the production and diffusion of relevant molecules, bacterial colonization rates, and particle interactions. This integrated approach expands the synthetic biology toolbox for EcN-based therapies, providing novel parts, circuits, and a model for tunable responses at inflammatory hotspots.

Keywords: engineered probiotic, IBD, inflammation, E. coli Nissle 1917 (EcN), nitric oxide, TNFα, nanobodies

Graphical abstract

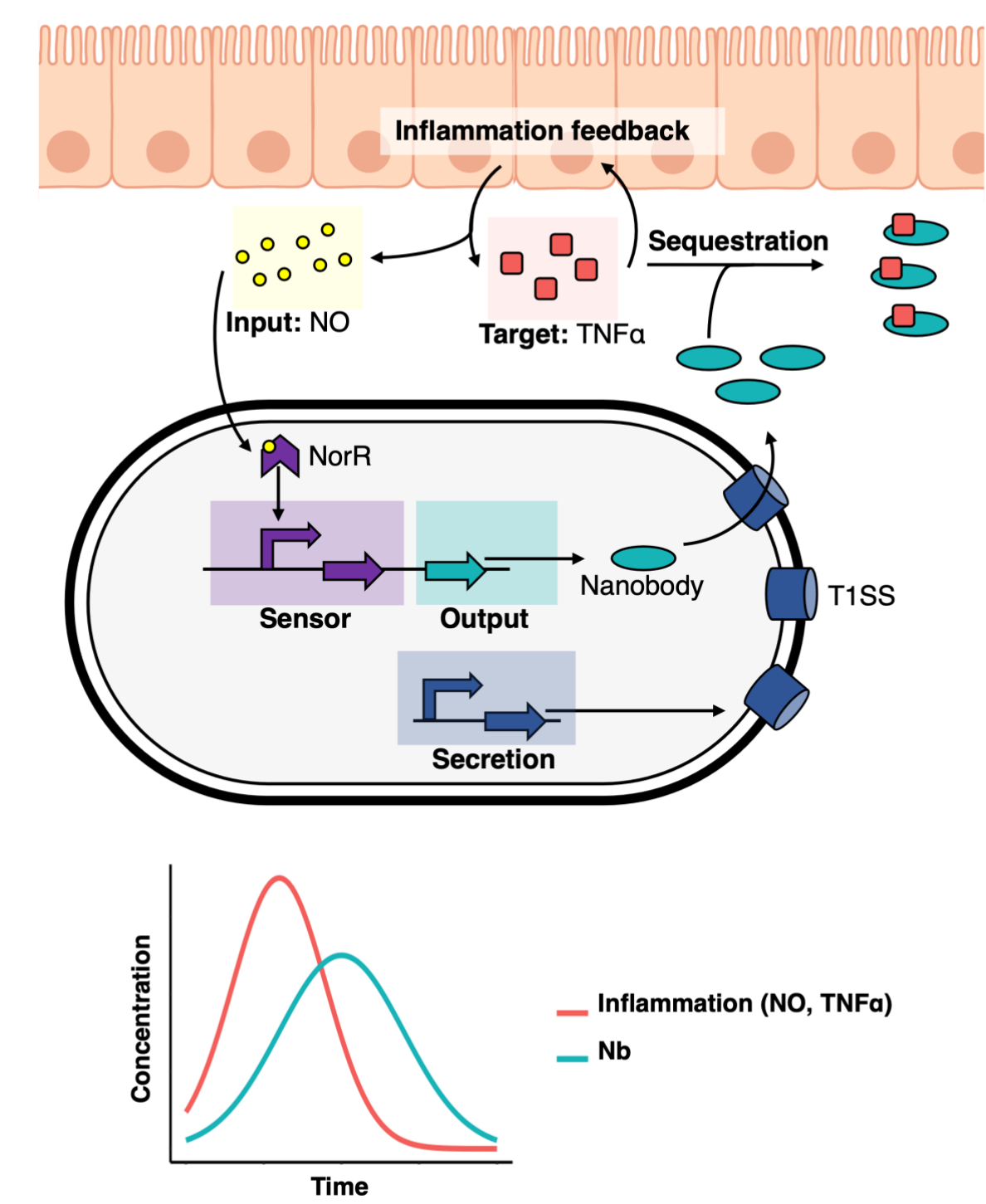

Graphical Table of Contents. **The engineered probiotic system**: Inflamed intestinal cells release the inflammatory regulator TNFα (depicted as red squares), which promotes inflammation through a positive feedback loop. Concurrently, these cells produce large amounts

of nitric oxide (NO, represented by yellow circles) during inflammation. Our custom-engineered EcN biosensor can detect NO using a NorR-based sensor (in purple) and subsequently trigger the production of nanobodies (in turquoise). These nanobodies are then released into the extracellular environment via a specially engineered secretion system in the bacterial host (shown in dark blue). Once outside the cell, the nanobodies attach to TNFα, effectively sequestering them and reducing inflammation. The graph at the bottom of this panel illustrates the general behavior of our system: nanobody production starts upon reaching a certain NO concentration threshold and continues in an NO-dependent fashion. As nanobodies are produced, they capture TNFα, leading to a reduction in inflammation and a decrease in NO production. This decrease in NO then halts the nanobody production.

INTRODUCTION

Inflammatory Bowel Diseases (IBD) are chronic relapsing inflammations of the gastrointestinal tract that affect more than six million people worldwide [1–5]. Inflammation of the intestinal mucosa compromises barrier function, exposing deeper gastrointestinal layers to luminal antigens and microbiota, which triggers aberrant immune responses and maintains local and systemic inflammation [2]. Current pharmacological interventions aim to induce clinical remission by reducing mucosal inflammation and alleviating disease symptoms.

Among the approved therapies for IBD[6], monoclonal antibodies against pro-inflammatory cytokines like tumor necrosis factor (TNFα), IL-12/23, or integrins are particularly effective [6]. TNFα is a key pro-inflammatory mediator with elevated levels in inflamed gut tissue[7], making it an attractive drug target with demonstrated therapeutic benefit [6,8,9]. However, the systemic action of these therapeutics can lead to immunosuppression, increasing the risk of serious infections and lymphoma [8,10]. Therefore, there is a high demand for new therapeutic solutions that target mucosal inflammation more precisely and are cost-effective [3,10,11].

Engineered probiotics[12,13] offer a potential solution for such treatments, being able to reach inflammatory hotspots in the gut where the mucus barrier is compromised by chronic inflammation [14]. The probiotic Escherichia coli Nissle 1917 (EcN) [15–17] is naturally present in the human gut and has been widely used to treat intestinal diseases due to its anti-inflammatory and antimicrobial properties [17–24]. Thus, EcN is a promising chassis for targeted gut therapies [25]. Over the last decade, this strain has been extensively engineered to produce biomolecules at disease sites, particularly for treating intestinal diseases [26–33]. However, despite recent developments in expanding the tools and biological parts for engineering EcN, there remains a

104 shortage of self-regulating genetic circuits that can recognize specific biomarkers and respond
105 by producing therapeutic molecules[34].
106
107 To address this challenge and contribute to the expansion of the EcN Synthetic Biology toolbox,
108 we designed, engineered, and characterized a new genetic circuit for EcN to act as a
109 biotherapeutic against gut inflammation. This circuit detects nitric oxide (NO) as a biomarker
110 and responds by producing and secreting nanobodies to sequester TNFα and locally reduce
111 inflammation. To date, only one other study has created a similar functional system, however,
112 without a biomarker-induced expression and using alternative components in their circuitry[33].
113 The scarcity of such systems in EcN highlights the need for alternative systems such as the one
114 presented in our study.
115
116 Nitric oxide is a free radical synthesized by inducible nitric oxide synthase in gut epithelial cells,
117 with increased concentrations at inflamed sites [35,36]. This small molecule can also penetrate
118 bacterial membranes without specialized surface receptors [37], making it an effective biomarker
119 for inflammation. In this study, we utilized a NO biosensor endogenous to *E. coli*, specifically
120 the NorR-pNorV system, which was previously modified and characterized by Xiaoyu J. Chen
121 et al.[38], to trigger the expression of the nanobody delivery system.
122
123 Nanobodies, single-domain antibodies that can bind specific antigens[39,40] , are advantageous in
124 therapeutic applications due to their superior tissue penetration, stability, and ease of production
125 by bacteria[33]. These nanobodies can be "humanized" to reduce immunogenicity by modifying
126 specific amino acids [41]. In this study, we used humanized nanobodies developed by Silence et
127 al. [42] , producing them for the first time in EcN.
128

The secretion of nanobodies is essential for TNFα inactivation since this cytokine is present in the gut extracellular environment. Most secretion systems in gram-negative bacteria such as EcN typically release proteins into the periplasmic space rather than the surrounding environment[43]. Thus, we utilized the Type I Hemolysin A Secretion System from uropathogenic *E. coli*[44–48]. This system has the advantage of being one of the smallest secretion complexes in gram-negative bacteria, and its functionality has not been described in EcN before.

Thus, in this study, we engineered a novel self-regulated system to produce and secrete anti-TNFα nanobodies in response to NO, aiming to reduce intestinal inflammation. Our data shows that although NO sensitivity was lower than reported in a previous study[38], our system successfully expressed a variety of humanized nanobodies in an inducible manner. We also demonstrate that the produced nanobodies can be effectively secreted to the extracellular environment, retaining their functional capabilities to bind TNFα and reduce inflammation in cell-based assays. This indicates that this system can also facilitate the screening and purification of nanobodies or other proteins of interest in future studies using EcN. Lastly, we developed a mathematical framework to investigate relevant parameters for gut inflammation treatment, addressing the scarcity of modelling tools for such systems.

RESULTS

Experimental design

We designed our system by integrating two independent modules on separate plasmids: a sensing module and a secretion module. The sensing module recognizes NO concentrations through the NorR transcription regulator and promotes the production of nanobodies in an inducible manner. The secretion module encodes a secretion system that allows the secretion of nanobodies into the extracellular environment. We characterized each component of our system independently before combining the complete engineered device. This allowed us not only to provide a proof of concept for each subsystem but also to optimize some of them in an iterative process. Firstly, we assessed different architectures of our sensing system through fluorescence reporter-based assays, characterizing their limit of detection and output fold-change in response to different NO concentrations. Secondly, we assessed the production and secretion of nanobodies and their activity using in vitro and cell-based assays. Finally, we tested the whole device and its ability to produce nanobodies in an induced manner. We complemented our study with a simple yet insightful mathematical framework assessing the interactions between the EcN and inflammation sites, focusing on the production rates of NO, the production rates of TNFα and the bacterial response to NO through production of the anti-TNFα nanobodies.

Characterization of the NO sensing module

To create an inducible system that can sense and respond to inflammation in the gut, we chose a NO-sensitive genetic circuit based on the NorR regulator. NorR is an endogenous transcription factor from *E. coli* responsible for sensing NO concentrations and modulating the expression of genes that are essential for NO detoxification under anaerobic conditions [49,50]. NorR interacts with NO through a non-haem iron center and binds cooperatively to three

enhancer sites at the pNorV promoter to regulate transcription of both *norVW* genes and its own divergently transcribed gene (*norR)* [49–51]. In *E. coli*, it thereby regulates the activity of the target *norV* gene in a NO-dependent manner. At low NO concentrations, NorR is predominantly present in its free form, which inhibits pNorV. However, at higher concentrations of NO, the radical binds NorR, inducing a conformational change of this protein, which makes it now able to promote σ54-dependent translational activation[52].

Our sensor was based on a previous study by Xiaoyu J. Chen et al.[38], consisting of the promoter pNorVβ, an optimized variant of the natural *E. coli K-12* pNorV lacking the second integration host factor (IHF) binding site [38]. We placed the promoter upstream a bicistronic operon containing genes encoding for a superfolder GFP (*sfGFP*)[53] and for the NorR regulator (*norR*), in this order. The regulatory logic is based on a positive feedback loop that modulates NorR availability in a NO-dependent manner [38] (**Figure 1a**, see **Supplementary Methods** and **Supplementary Figures S1-S3** for more information about constructs and plasmids). This architecture ensures low inhibitory NorR levels in the cells but high availability of activated NorR in environments with a high NO concentration [38]. Due to the potential cellular toxicity of NO[54], we verified that the concentrations used did not influence EcN cell growth in our experiments (**Supplementary Figure S4**). Removal of the positive feedback loop decreases the induced expression of downstream genes (see **Supplementary Figure S5**). To characterize and compare our NO-sensing constructs` limit of detection and dynamic range, we performed time-lapse fluorescence plate reader assays. We performed these experiments using EcN cells.

We observed that the NorR circuit design with the best performance in the original study[38] featured three consecutive ribosome binding sites (RBSs) upstream of the *sfGFP* gene. To investigate the impact of altering the number of consecutive RBSs on the sensitivity of our system, we designed, constructed, and characterized three variants with one, two, or three

198 consecutive RBSs, respectively named β-1, β-2, and β-3 (**Figure 1b**). This approach allowed
199 us to assess the effect of varying the number of RBSs on the sensitivity of our system. To
200 account for background fluorescence, we systematically compared our constructs to a negative
201 control plasmid that did not contain any promoter (**Figure 1b**). We also compared our constructs
202 to the wild-type pNorV with a single RBS (**Figure 1b**).
203
204 **The number of Ribosome Binding Sites (RBSs) upstream of *sfGFP* influences its**
205 **expression levels and the leakiness of the construct**
206 Our first observation was that the pNorVβ system exhibited higher fluorescence levels than the
207 wild-type, regardless of the NO concentration (**Figure 1c**), indicating this system is leakier than
208 the wild-type. By changing the number of RBSs, we observed differences in our detection limits
209 and the overall fluorescent reporter expression. We can observe in **Figure 1c** that our constructs
210 can be increasingly ranked regarding basal sfGFP expression as WT < β-1 < β-3< β-2.
211 Interestingly, the consecutive addition of ribosome binding sites (RBSs) does not result in a
212 linear increase in sfGFP expression. We speculate that this phenomenon may be due to
213 structural consequences arising from repeating sequences in tandem, such as the potential
214 formation of secondary structures or hairpins [55]. Additionally, ribosome stalling could occur,
215 where ribosomes pause or slow down due to interactions between ribosomes initiated at
216 different RBSs[56,57].
217
218 We observed that β-2 is highly leaky, showing higher sfGFP expression even in the absence of
219 induction ([NO] = 0). The higher expression baseline of β-2 sfGFP expression can also be
220 highlighted in **Figure 1d,** showing the fold-of change in sfGFP expression for each construct
221 at all tested NO concentrations. We also observed in **Figure 1d** that β-1 responds to a lower
222 concentration than the other constructs ([NO] = 125μM). This is further illustrated in **Figure**
223 **1e**, which shows the rate of change, a sensitivity metric for each genetic construct to variations

in NO levels, as measured by changes in sfGFP fluorescence. The percentage change in sfGFP fluorescence intensity is calculated when the NO concentration shifts from an initial baseline to a new value. This percentage is then normalized against the initial NO concentration, providing a relative measure of change.

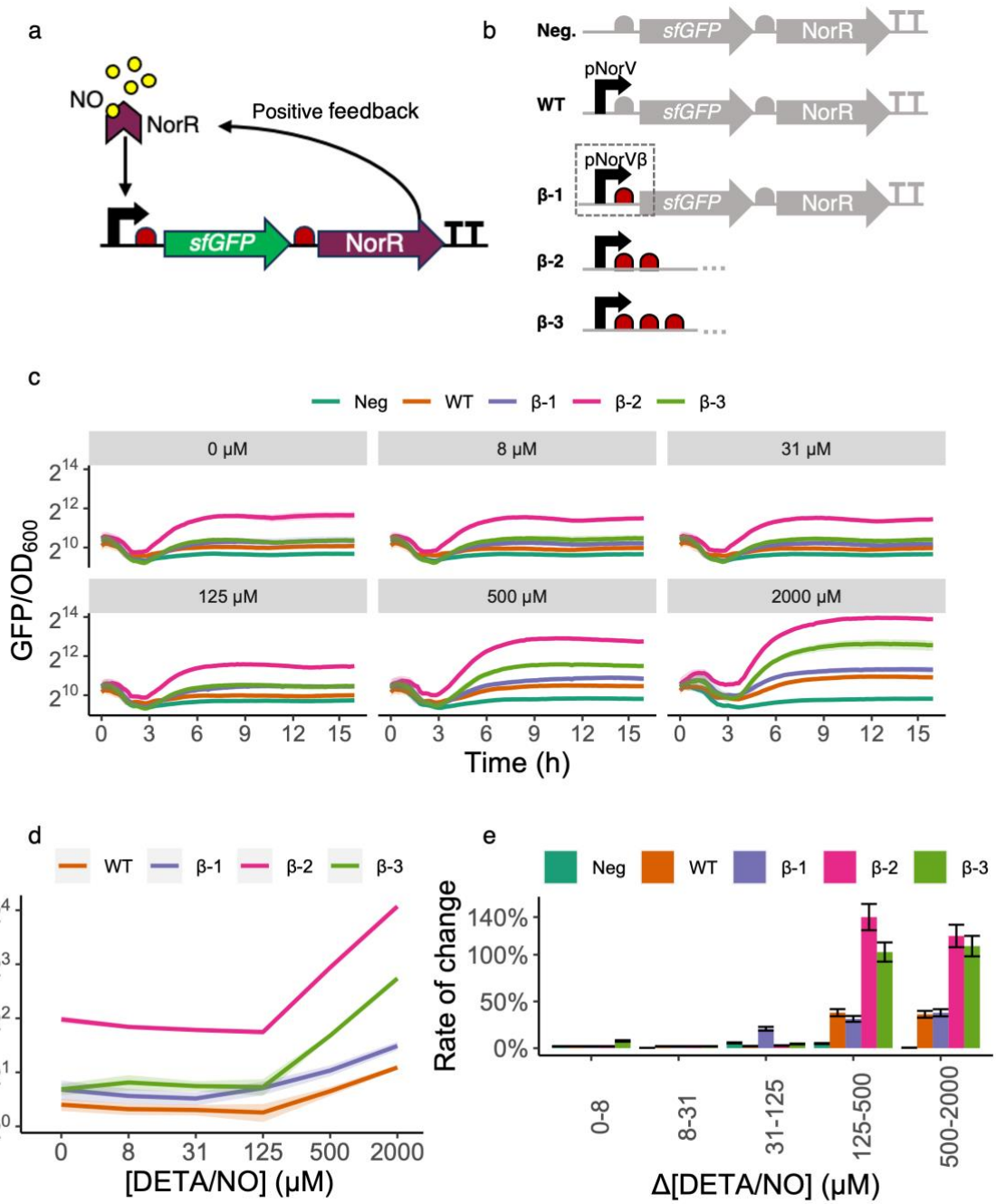

Figure 1. Design and characterization of the NO detection module. a. NO-dependent activation from NorR. The NorR transcription factor (represented by the purple chevron)

binds its cognate binding site at the promoter pNorVβ (black arrow). When not bound to nitric oxide (yellow circles), NorR acts as a competitive inhibitor of its NO-bound form and represses pNorVβ. However, at high NO concentrations, the NO-bound form of NorR is predominant and acts as a positive inducer of pNorVβ. The presence of *norR* in the inducible operon generates a positive feedback mechanism. Ribosomes are represented in red and the *sfGFP* gene in green. **b. Construct variants characterized.** Our original construct β-1 consisted of *sfGFP* and *norR*, preceded by one RBS each, and placed under the control of the optimized promoter pNorVβ. To avoid read-through, we placed a double-terminator at the end of the operon. We normalized the responses of β-1, β-2, and β-3 to a negative control (Neg) and compared to a positive control (WT). Neg consisted of *sfGFP* and *norR* genes, preceded by one RBS each, and did not contain any promoter, accounting for the intrinsic leakiness of our module. WT consisted of *sfGFP* and *norR* genes, preceded by one RBS each, and placed under the control of the wild-type promoter pNorV.) **c. Time-lapse fluorescence assay for construct characterization.** We have grown each construct for 16 hours (x-axis) on a microplate reader where green fluorescence (arbitrary units) and measured the culture's OD_{600} every 15 minutes. The y-axis represents normalized fluorescence values (sfGFP/OD_{600}). Each panel grid represents a different concentration of diethylenetriamine/nitric oxide (DETA/NO) used to test individual constructs. The DETA/NO gradients we used were 0, 8, 31,125,500, and 2000μM. Each line color represents a construct. Line shadings represent the standard deviation of our biological replicates ($n=3$). We performed all measurements with both biological and technical triplicates. Notice that measurements are on $\log_2$ scale to facilitate data visualization. **d. Fold of change for each construct.** Each curve represents the fold of change for each construct at T = 8h along a gradient of NO concentrations. Line shadings represent the standard deviation of our biological replicates ($n=3$). Notice that measurements are on the $\log_2$ scale to facilitate data visualization. **e. Rate of change for each construct.** The bar plots represent the rate of change for each construct for each DETA/NO change of concentration at T = 8h. We calculated rates

of change as the relative increase in fluorescence (reported as percentages, y-axis) from an initial NO concentration to the next incremental one. We have performed such calculations for each consecutive pair of concentrations (x-axis). Error bars represent the standard deviation of our biological replicates (*n=3*).

Purified monovalent and bivalent anti-TNFα nanobodies efficiently capture TNFα, comparable to monoclonal antibodies used in the clinics.

To develop the nanobody production module, we have selected three previously described anti-TNFα humanized nanobody candidates[42] and combined these to additionally produce bivalent nanobodies, linked via a short peptide linker (EPKTPKPQPAAA; for monovalent and bivalent nanobodies **see Materials and Methods Table 3**). Firstly, to assess the proper expression and activity of our candidates, we cloned their sequences into the pSBinit[58] expression vector (**see Materials and Methods, Table 2 and Supplementary Figures S6-S7**), allowing controlled expression upon L-arabinose induction (**see Figure 2a**). We transformed the plasmids into the expression strain *E. coli MC1061* (**see Materials and Methods, Table 1**). After induction, we performed periplasmic extraction for monovalent nanobodies and whole-cell lysis for bivalent constructs (**Figure 2a**) and observed a quantitatively higher output of monovalent nanobodies compared to the bivalent constructs (**Supplementary Figures S8-S9**).

We proceeded by performing an ELISA with the purified nanobodies to test their capability to bind TNFα (**see Materials and Methods**). The **Figure 2b** shows the fold change in the binding capacity of our different nanobody candidates compared to our negative control. The bivalent nanobodies exhibit a statistically significant enhancement in binding efficiency, demonstrating an average 1.3-fold increase over the monovalent nanobodies (see **Supplementary Figure S10**). The bivalent constructs show a mean TNFα binding capacity of 13.5 ± 0.1 (mean ± s.d.), compared to 12.3 ± 0.2 for the monovalent constructs. Adalimumab, an approved monoclonal

283 anti-TNFα antibody that is already used in the clinic to treat IBD (see **Materials and Methods**
284 for antibody purification), is used as a positive control and our bivalent nanobody constructs
285 show a similar binding capability to this therapeutic.
286
287 **Anti-TNFα nanobodies show anti-inflammatory effects on stimulated human monocytes**
288 **in vitro**
289 To evaluate the effect of anti-TNFα nanobodies on the immune response of cells to an
290 inflammatory stimulus in vitro, we stimulated THP-1 human monocytes with increasing
291 concentrations of recombinant TNFα (rTNFα) and subsequently added our purified nanobody
292 candidates (**see Materials and Methods**). We performed real-time quantitative PCR analysis
293 and measured the relative amount of *IL1B* expressed by immune cells as a response to
294 inflammation through TNFα signaling (**Figure 2c**, **Supplementary Methods**). The cytokine
295 IL-1β is an important inflammation mediator and, therefore, a good marker to prove functional
296 TNFα-inhibition[59].
297
298 We were able to observe an up to 4-fold decrease in *IL1B* expression of stimulated monocytes
299 when different nanobodies were added compared to the control cells that only received the
300 inflammatory stimulus (**Figure 2d**). This experiment shows that tested nanobodies have the
301 same capability to lower inflammation as monoclonal antibodies, which are already used in the
302 clinic to treat IBD patients. However, with increasing TNFα concentrations, the anti-
303 inflammatory effect that the nanobodies have on the monocytes seems to slowly decline,
304 indicating that higher concentrations of nanobodies are required to maintain low *IL1B*
305 expression levels. This decline is not observable with the available drug Adalimumab[60]. It is
306 also important to note that the difference between monovalent and bivalent nanobody constructs
307 does not seem to be of great influence on the inflammatory response of triggered monocytes.

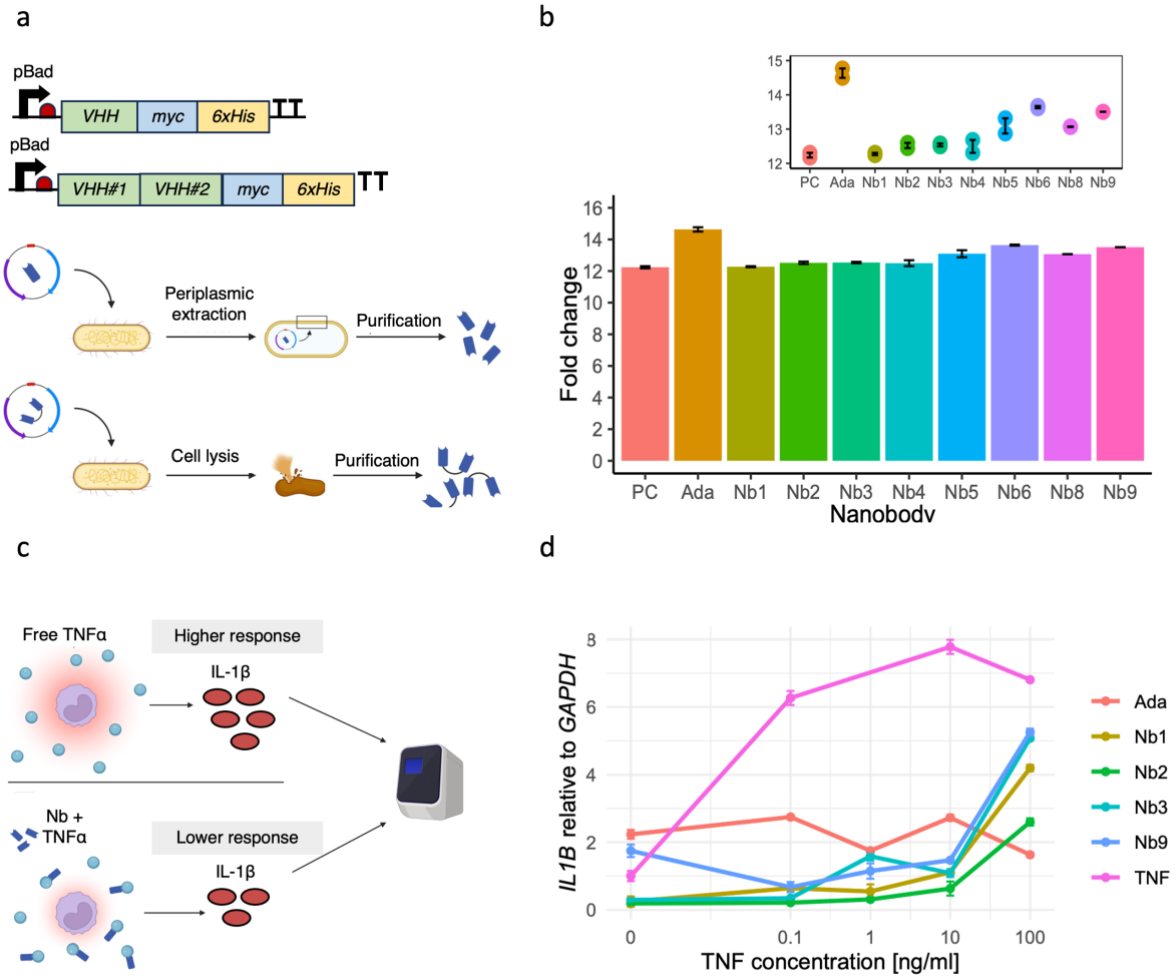

Figure 2. Design and characterization of the purified anti-TNFα nanobodies. a. Design of monovalent and bivalent anti-TNFα nanobodies. We linked bivalent nanobody constructs via a short peptide linker (EPKTPKPQPAAA). To characterize the nanobodies, we added a myc-tag and a his-tag to their C-terminal sites. Their expression was under the control of the inducible pBad system, which relies on the addition of L-arabinose. We induced the expression of nanobodies with the pBad inducible system. We harvested monovalent nanobodies via periplasmic extraction and bivalent nanobodies through whole-cell lysis. We purified all nanobodies by immobilized metal anion chromatography (IMAC). **b. Testing binding capability of purified nanobodies with enzyme-linked immunosorbent assay.** We tested TNFα-binding using an ELISA by capturing the purified nanobodies via their myc-tag. Then, we visualized the binding of nanobodies to biotinylated TNFα with the streptavidin-peroxidase.

We measured the absorbance of each well with a plate reader and analyzed the fold change with R studio. **c. Principle of the cell assay used to determine anti-inflammatory properties of purified anti-TNFα nanobodies.** We incubated Human THP-1 monocytes with rTNFα and different purified anti-TNFα nanobodies. We assessed the immune response of the monocytic cell line to rTNFα by quantitatively determining the *IL1B* expression levels with the use of RT-qPCR. The binding of the nanobodies to rTNFα is supposed to inhibit the inflammatory effect observed in untreated but stimulated THP-1 cells. **d. *IL1B* expression compared to *GAPDH* in human THP-1 monocytic cell line.** Quantitative analysis of the inflammatory *IL1B* expression levels revealed a decreased immune response of rTNFα-stimulated cells when purified nanobodies were added, compared to untreated cells (labeled as "TNF", pink line). Adalimumab is an anti-TNFα monoclonal antibody frequently used in the clinic to treat IBD patients and served in this experiment as a positive control.

Anti-TNFα nanobodies can be secreted from *EcN*

In order for EcN to deliver nanobodies to its environment, it must be able to secrete them without impacting their function. To achieve this, we engineered the HlyA secretion system[47,48] into EcN along with fusing the nanobodies to the HlyA-tag, marking them for selective export (**Figure 3a, Supplementary Figure S11**). As a first step, we tested the functionality of the nanobodies after expression and secretion in *E. coli MC1061*. We performed a double transformation of *E. coli MC1061* with two plasmids: our secretion plasmid (**Supplementary Figure S11**) and the pSBinit expression plasmid, which allows for nanobody expression upon L-arabinose induction (**Supplementary Figure S7**). After overnight induction, we harvested the supernatant from the cell culture, and performed a western blot and ELISA to quantify the presence and TNFα binding of the secreted nanobodies (**Figure 3b**). In EcN, the nanobody Nb1 and the bivalent nanobody Nb8 were successfully secreted, and their binding affinities were maintained (**Figure 3c,** (**Supplementary Figures S13-S14**).

346 **Nitric oxide can be used to trigger anti-TNFα nanobody expression**

347 To create a system capable of sensing NO and thereby triggering the production and secretion
348 of nanobodies, we built a new plasmid, where the monovalent nanobody Nb1 was cloned
349 downstream of the aforementioned pNorVβ promoter (see **Table 2**, **Supplementary Methods**
350 **and Supplementary Figure S15**). We used the circuit with two RBS (ß-2) upstream of the
351 cloned nanobodies, as it presented the highest expression levels. We used DETA/NO for
352 induction and allowed cells to express nanobodies overnight. We then quantified the presence
353 of nanobodies in the supernatant by western blot, in which we detected secreted nanobodies
354 using a C-terminal myc-tag. The western blot showed that while EcN could sense NO and
355 increase the expression and secretion of anti-TNFα nanobodies, there was still a high-level
356 baseline expression without NO (**see Supplementary Figure S16**).
357
358 Despite the high levels of baseline expression, the secreted nanobodies maintained their
359 functionality, as shown in ELISA assays (**see Supplementary Figure S16**). To reduce baseline
360 expression, we tested an alternative circuit differing by having a single RBS (ß-1) upstream of
361 the nanobody coding region. This had previously shown less expression leakage. The single
362 RBS system yielded a more dynamic response to NO concentration in *E. coli* MC1061 after 8
363 hours of expression. Relative expression showed a threefold increase from baseline to a 1 mM
364 NO concentration (**Figure 3d**). It is worth noting that we observed a basal production of
365 nanobodies even without the addition of the NO inducer (**Figure 3d, rightmost western blot**
366 **and its corresponding bar plot**). Lastly, the control with no secretion system shows no
367 presence of nanobodies in the supernatant. This confirms the need for a secretion system to
368 export the nanobodies, as cell death does not appear to result in the release of functional
369 nanobodies.

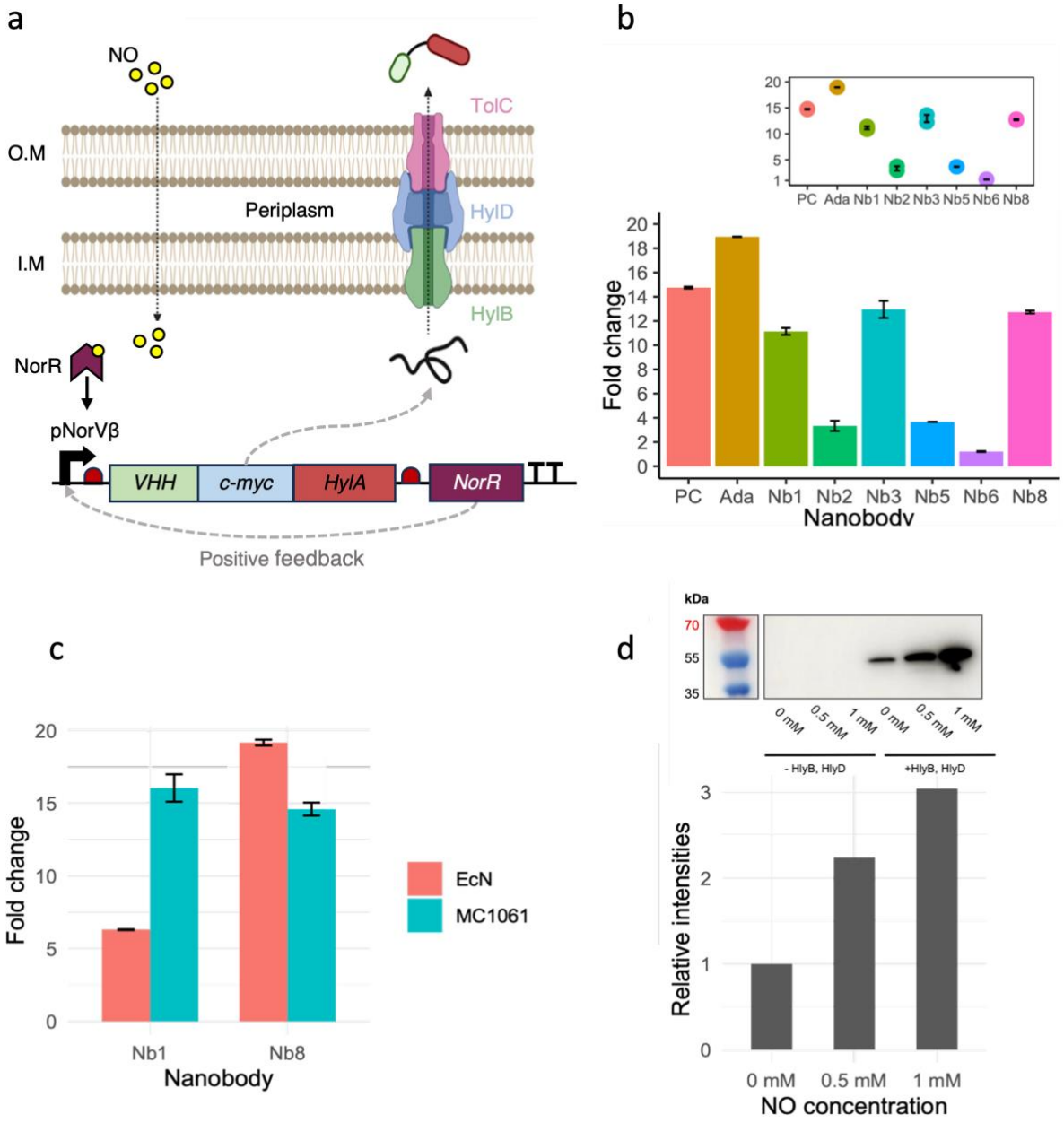

Figure 3. Design and characterisation of arabinose- and NO-induced anti-TNFα nanobodies secretion in *E. coli Nissle 1917* and *E. coli MC1061*. a. Principle of NO-induced nanobody secretion with the Hemolysin A secretion system. Nitric oxide is a small organic molecule able to surpass the double membrane of *E. coli*. NO binding to the PnorV-ß promoter induces the expression of the monovalent nanobody candidate Nb1, which is tagged with a myc- and HlyA-tag. NorR expressions result in a positive feedback loop, enhancing the nanobody expression further. Thanks to the HlyA-tag, the produced nanobodies are secreted by

the hemolysin A secretion system in a one-step manner into the extracellular space. **b. Arabinose-induced secretion of monovalent and bivalent nanobodies with *E. coli MC1061*.** Western blot and ELISA analysis revealed successful secretion of functional monovalent and bivalent nanobodies upon overnight arabinose induction in *E. coli MC1061*. **c. Arabinose-induced secretion of monovalent and bivalent anti-TNFα nanobodies in *EcN* and *MC1061*.** ELISA analysis shows a successful secretion of functional monovalent Nb1 and bivalent Nb8 nanobodies upon overnight arabinose induction, retaining their TNFα-binding capabilities regardless of the HlyA-tag. **d. NO-induced secretion of monovalent anti-TNFα nanobodies with a single-RBS system in *E. coli MC1061*.** The NO-induced monovalent nanobody secretion was achieved using the single-RBS system (ß-1). This yielded a more dynamic response to NO than the previous two-RBS system (ß-2) (**Supplementary Figure S16**) and a lower baseline expression of monovalent nanobody candidate Nb1 in *E. coli MC1061*. The absence of the two secretion system components (HlyB and HlyD) resulted, as expected, in no secretion of nanobodies. With increasing NO-levels, higher nanobody expression can be observed. A baseline expression in the absence of NO is still present yet weaker than in the ß-2 system (**Supplementary Figure S16**).

A coarse-grained model for engineered probiotics in the gut

To support the experimental claims, we constructed a two-dimensional lattice-based reaction-diffusion model [61–65] of the gut environment, as in-vivo testing in the gut microbiome is outside the scope of this study. The model is illustrated in **Figure 5a**.

The model's primary objective was to examine the interactions between EcN and inflammation sites in a simplified manner, specifically focusing on the NO concentrations[66], the production rates of TNFα[67] and the bacterial response to NO through the production of the TNFα-binding nanobodies [68]. Model methods and an in-depth description of the parameters used can be found

in the model section of the appendix. Through cycles of diffusion, decay, and reemission, we provided a preliminary outlook on the efficacy of our proposed treatment and its potential for healthcare applications. We note that the model is a coarse-grained one, and faithfully representing the gut environment was out of its scope. We focused on identifying the crucial parameters to tune in future work to optimize the treatment before heading into a further testing stage.

To favor interpretability, generalization, and to promote ease of access and collaboration, the model follows a simplicity-based design. The model interprets a $1 mm^2$ area of the gut surface as a 2D grid, with each grid cell representing a $1 \mu m^3$ volume, containing the local concentration values for each parameter. The model operates in discrete time steps, with adaptations to make it approach a continuous time scale.

Estimating the minimum number of bacteria for effective treatment

To get an overview of the importance of the different parameters, we performed a series of simulations where we swept two variables at the same time over the range of our expected values and simulated for 60-second time steps.

In our first series of simulations, illustrated in **Figure 5b**, we estimated the minimum number of bacteria needed to provide effective treatment and evaluated the densities on a great range of biologically plausible TNFα concentrations. The results show that around 20 bacteria per mm^2 should be enough to cover the inflamed gut area and sufficiently combat the inflammation for the expected TNFα concentrations. For higher concentrations of TNFα, however, the nanobodies produced are not sufficient to combat inflammation, and larger bacterial populations are needed. The graphs suggest a rough relationship of a doubling in bacterial density being able to combat a magnitude higher TNFα concentration. Bacterial density

estimates place this requirement at a feasible replacement value of 20 out of 10^4 gut bacteria per mm² [69,70] and thus the required colonization should be feasible and in further experiments we assume that this threshold will be reached. In **Figure 5e**, we investigate whether increasing the nanobody production could also be a viable solution.

Nitric oxide detection threshold and nanobody production:

In our study, the threshold for NO detection, the minimum amount of NO required for nanobody production, is essential for ensuring an inflammation-dependent response. In **Figure 5c,** we evaluated a range of these sensing thresholds and the amount of TNFα at the inflammation sites. As our threshold closely aligns with the expected NO concentration of around 15 μM[36] (**for details, see Supplementary Methods and Supplementary Figure S17**), even slight decreases in sensitivity lead from the absence of inflammation reduction to complete reduction, even with higher than expected amounts of TNFα. Increased sensitivity of the bacteria towards NO gives diminishing returns, as this mostly affects bacteria in edge regions that detect trace amounts of NO but do not produce nanobodies at the affected location. In turn, there will be an excess production of nanobodies in these regions that hardly contribute to combating inflammation. It is important to note that in our simulations, we kept the amount of NO produced at inflammation sites constant, even for higher TNFα concentrations. In a patient setting, however, NO levels might vary significantly.

Comparison between bacterial number and nanobody production:

In **Figure 5d**, we assessed the importance of the number of bacteria we can introduce against the nanobody production of a single bacteria. For our expected TNFα values, the number of bacteria has a far greater effect than the amount of nanobodies produced per bacteria. This is most likely due to the nanobodies being spread locally, and even at the same amount of net nanobodies produced, greater coverage of gut-inflamed areas ensures that the nanobodies are

produced where they need to be. This trade-off also guarantees that no excess amount of nanobodies is produced which could lead to possible side effects. In vivo testing is required to assess the actual viability of our engineered bacteria, and further optimization should be based on this.

In **Figure 5e**, we investigate whether higher TNFα concentrations can be mitigated by increasing nanobody production. The results demonstrate that, with a bacterial density of at least 20 per mm², an increase in nanobody production effectively reduces TNFα levels. However, this effect is less pronounced compared to increasing the number of bacteria, as shown in **Figure 5b**, which more effectively reduces even higher concentrations of TNFα. Nevertheless, increasing nanobody production might be easier to achieve and still offers a viable approach to combating elevated TNFα concentrations.

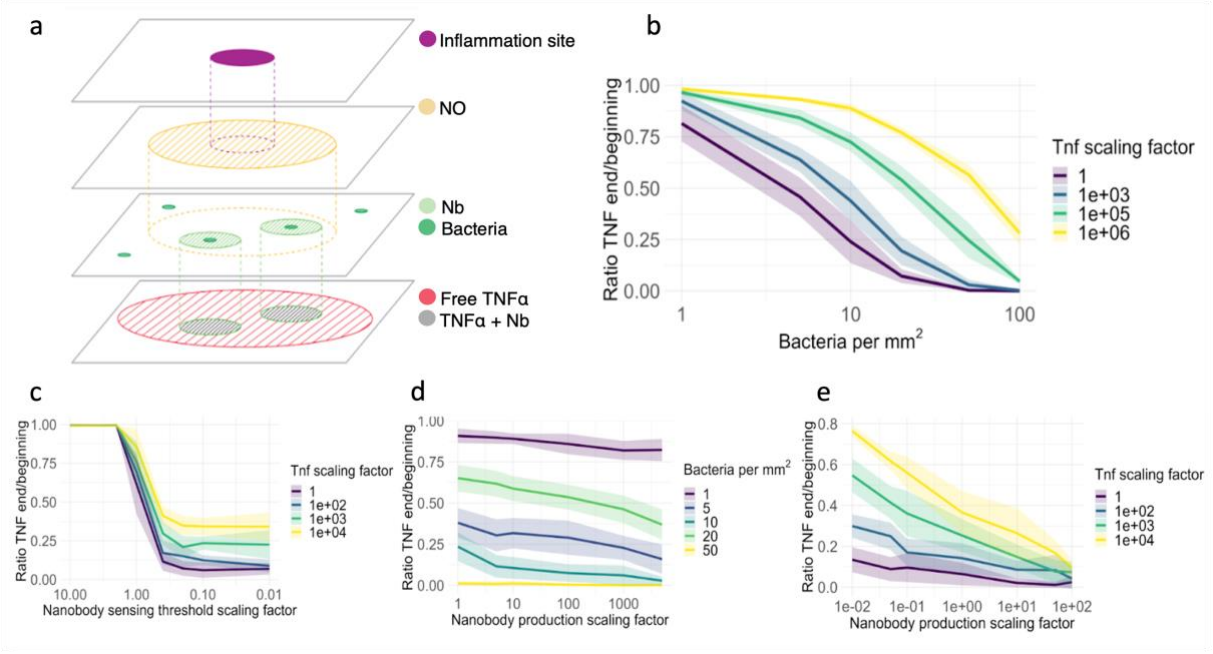

Figure 4. **The reaction-diffusion model was evaluated on key parameters.** The model's purpose was to explore which parameters could be essential for the efficacy of our system. Parameters that are not varied are set to their default value, except for the sensing threshold, which we decreased by a factor of 10 during simulations as done in a recent study[38], for

visibility reasons. We simulated each parameter configuration 10 times. Line shadings represent the standard deviation. **a. Illustration of the components of the reaction-diffusion model. b. Relationship between bacterial density and TNFα concentrations. (n = 240). c. Relationship between sensing threshold and TNFα concentrations. (n=280) d. Relationship between nanobody production and bacterial density. (n = 300) e. Relationship between nanobody production and TNFα concentrations. (n = 380)**

DISCUSSION

Here, we describe the development of an integrated molecular system in EcN for the local sensing of gut inflammation and the production/delivery of high-specificity effectors to mitigate such inflammation. Specifically, we have engineered both laboratory and non-pathogenic/probiotic human *E. coli* strains with a coupled system that can secrete nanobodies in a regulated manner upon NO induction. Secretion is achieved through the adoption of an exogenous Type I Hemolysin A Secretion System, which has been characterized in EcN for the first time in this study. We have also characterized a new library of humanized nanobodies in EcN, demonstrating that they can be successfully secreted and retain their functionality in vitro and in cell assays, binding to TNFα as efficiently as conventional drugs used for targeting this pro-inflammatory molecule. Modularity is a key strength of our system. The regulator can be easily swapped, allowing the detection of different biomarkers[27,34]. The cargo (nanobody in our case) can also be replaced in a straightforward manner with other therapeutic proteins, such as small peptides and colonization-increasing factors.

Although mathematical models regarding gut colonization are available[71–75], they are mostly focused on host-pathogen interactions and not on the colonization-sensing-delivery process from engineered probiotics. Thus, we also developed a simplified yet insightful modelling framework to investigate relevant parameters on probiotic engineering and its subsequent colonization in the gut. Specifically, we investigated the interactions between the probiotic bacteria and inflammation sites, focusing on biomarker (NO) concentration detection thresholds, therapeutic molecule production rates (TNFα), and the bacterial response in terms of therapeutic-target interactions (nanobody-TNFα). We observed that approximately 20 bacteria per mm^2 are sufficient to manage inflammation. Bacterial density estimates place this requirement at a feasible replacement value of 20 out of 10^4 gut bacteria per mm^2 [69,70]. However,

at higher TNFα levels, increased bacterial densities are necessary, suggesting a rough doubling of bacterial density for each magnitude increase in TNFα concentration.

The current understanding of nitric oxide concentrations at inflammation sites within the gut across various patient demographics is limited, with most data focused on serum concentrations [36]. It is estimated that a baseline concentration of around 14 μM NO is typically necessary to detect gut inflammation [36]. However, we anticipate that the luminal NO concentrations in the gut, particularly at sites of active inflammation, are likely to be considerably higher than this threshold. This expectation is based on the fact that NO, with its notably short half-life and rapid diffusion rates within the body[76,77], would be more concentrated in regions immediately adjacent to inflammation sites. In light of the scarce available data on serum NO concentrations [36], our simulations suggest that an optimal concentration for nanobody production in response to NO is approximately 15 μM. We also observed that enhancing bacterial sensitivity to NO beyond this threshold may lead to diminishing returns. Specifically, this could result in the overproduction of nanobodies in peripheral areas, where they might not contribute effectively to inflammation reduction.

When comparing the impact of the bacterial number on nanobody production per bacterium through simulations, our results indicate that the number of bacteria plays a more critical role than the number of nanobodies produced by each bacterium. This is likely due to the localized distribution of nanobodies, suggesting that a broader gut coverage by bacteria is more effective than increasing the production rate of nanobodies per bacterium. This balance is crucial to avoid the production of excess nanobodies, which could lead to potential side effects and metabolic burden on the bacterial host[78–80]. We highlight that a mathematical model is an oversimplification of reality and does not capture many complexities of the in vivo environment. Future developments in our modelling approach should include important variables such as the

consequences of gene expression noise (heterogeneity in gene expression)[81,82], the reevaluation of the assumptions regarding gut geometry, an enhancement of the diffusion model to encompass three dimensions and the consequences of microenvironmental gut conditions on bacterial growth[83]. Moreover, conducting in vivo studies of the treatment will be instrumental in refining the model as this iterative process of model refinement is essential for advancing our understanding of engineered probiotics[84,85].

The experimental characterization of our NorR-based circuit revealed that the NO detection threshold in our constructs was higher than the one reported in the original study where this circuit was designed [38]. This discrepancy could stem from several factors. Firstly, the plasmid used in our experiments differed from that in the referenced study [38] , and we were unable to access the complete sequences of their constructs, which may have influenced our results. Additionally, our experiments were conducted under aerobic conditions. Previous research has shown that anaerobic environments, akin to the gut's natural state, can decrease the NO detection threshold of the NorR system by at least five-fold, due to interactions between oxygen and the iron center of NorR [49] . Consequently, while our sensor system in EcN has been characterized and improved under aerobic conditions, there is substantial potential to enhance its sensitivity to lower, more physiologically relevant NO concentrations. Future studies could achieve this through advanced protein and promoter engineering techniques (e.g., directed evolution and combinatorial designs coupled with fluorescence-based screening methods [86–89]) and by transitioning to anaerobic assays.

We highlight that although our results support the potential of our system for biotherapeutic applications, the transition from test tubes to translational applications faces many challenges[90–93], from consistent therapeutic delivery methods to the long-term maintenance of engineered bacteria in the gut. The stable colonization of engineered probiotics in the gut can be negatively

558 impacted by metabolic burden—the allocation of resources towards the engineered system—
559 which can hinder bacterial growth in the complex microbiome environment[79]. Moreover,
560 evolutionary changes might disrupt circuit functionality over short time periods [94]. The
561 heterogeneity in bacterial expression due to background genetic mutations or expression noise
562 might also lead to variability in treatment efficacy[94]. Additionally, the interactions between the
563 host immune system and engineered probiotics require thorough investigation to ensure long-
564 term efficacy and safety [95,96]. To address some of these challenges, strategies such as integrating
565 the genetic circuit into the genome can enhance the stability and robustness of the device's
566 functionality[78,94]. Combining whole-cell and host-microbiome metabolic models with in vivo
567 assays of viability and prevalence of engineered probiotics is also important for predicting the
568 long-term maintenance of such systems [93,97–101]. Moreover, incorporating antibiotic resistance-
569 free plasmids [102] and containment modules [93,103] is important to prevent the unintended spread
570 of engineered bacteria and antibiotic resistance genes.
571
572 Despite the aforementioned challenges, Synthetic Biology is rapidly transitioning from
573 laboratory experiments to tangible, real-world applications[104–106]. In 2019, ZBiotics Company,
574 USA, pioneered this field by being the first to produce and sell genetically engineered probiotic
575 products, marking the beginning of a burgeoning industry. In a recent notable study, researchers
576 developed a novel system within EcN (PROT3EcT) and validated it in an animal model [33]. They
577 demonstrated effective colonization of the mouse gut with constitutive production of
578 nanobodies targeting TNFα, resulting in localized inflammation mitigation. Although our
579 system employs different components—specifically, a biomarker-dependent sensing module,
580 distinct nanobodies, and an alternate secretion system—their results are highly encouraging,
581 suggesting the potential functionality of our system in animal models. In this rapidly
582 progressing landscape, our study focused on providing new parts, a new modular system, and

583 a mathematical framework to expand EcN's Synthetic Biology toolbox and support ongoing
584 efforts in the probiotic engineering community.
585
586 **MATERIALS AND METHODS**
587
588 **Media and buffers**
589 M9 medium is advantageous due to its low cost, low auto-fluorescence (when excited at 488
590 nm), and low absorbance. We used M9 medium, supplemented with specific amino acids or
591 other metabolites (such as thiamine or casamino acids), for experiments measuring sfGFP
592 fluorescence to ensure minimal auto-fluorescence and absorbance of the samples. To prepare a
593 50 mL volume of M9 medium, we added the reagents in the following order: 10 mL of M9 salt
594 (5x), 100 µL of MgSO4 (1M), 50 µL of CaCl2 (0.1M), 1.5 mL of Cas Aa (2%), and 1 mL of
595 Glucose (20%), then added water to reach a final volume of 50 mL. If necessary, we
596 supplemented M9 medium with the appropriate antibiotic at a 1:1000 ratio. We conducted all
597 preparation steps under sterile conditions.
598

599 **Table 1. List of bacterial strains used in this study:**

Name	Genotype	Selective antibiotics	T, °C	Description
E. coli Nissle 1917	Unavailable	None	37°C	First described on[15,16]. Obtained from Mutaflor® (Herdecke, Germany)
E. coli MC1061	F⁻*hsd*R(r_K–, m_K+) *ara*D139 Δ(*ara*ABC-*leu*)7679 *gal*U *gal*K Δ*lac*X74 *rps*L(StrR) *thi* *mcr*B / P3: Kan^R Amp^R (am) Tet^R (am)	Streptomycin, Kanamycin, Ampicillin, Tetracycline	37°C	Commercially obtained from Thermofisher (C66303)
E. coli Mach1	F⁻ φ80*lac*ZΔM15 Δ*lac*X74 *hsd*R(r_K–, m_K+) Δ*rec*A1398 *end*A1 *ton*A	None	37°C	Commercially obtained from Thermofisher (C862003)

600

601 **Table 2. List of plasmids used in this study:**

Name	Description
piGEM1	This study. Negative control. Encodes for *sfGFP* and *norR*, does not contain any promoter.
piGEM3	This study. Encodes for *sfGFP* and *norR* under the control of the already characterized inducible promoter pNorV.
piGEM2.1	This study. Encodes for *sfGFP* and *norR* under the control of the inducible promoter pNorVβ. This construct contains 1 RBS directly upstream of *sfGFP*.
piGEM2.2	This study. Encodes for *sfGFP* and *norR* under the control of the inducible promoter pNorVβ. This construct contains 2 RBS and a spacer upstream of *sfGFP*.
piGEM2.3	This study. Encodes for *sfGFP* and *norR* under the control of the inducible promoter pNorVβ. This construct contains 3 RBS and a spacer upstream of *sfGFP*.
piGEM2.2N	This study. Encodes for *sfGFP* under the control of the inducible promoter pNorVβ. This construct contains 2 RBS and a spacer upstream of *sfGFP*. This construct does not contain *norR*.
pSBinit	Retrieved from [58], Addgene #110100. E.coli entry and expression vector for FX cloning system, N-terminal pelB signal sequence and C-terminal myc and 6xHisTag
purNb1	This study. Nanobody candidate VHH#2B cloned into pSBinit expression vector via FX cloning
purNb2	This study. Nanobody candidate VHH#3E cloned into pSBinit expression vector via FX cloning
purNb3	This study. Nanobody candidate VHH#12B cloned into pSBinit expression vector via FX cloning
purNb4	This study. Nanobody candidate VHH#2B-VHH#2B cloned into pSBinit expression vector via FX cloning
purNb5	This study. Nanobody candidate VHH#3E-VHH#3E cloned into pSBinit expression vector via FX cloning
purNb6	This study. Nanobody candidate VHH#12B-VHH#12B cloned into pSBinit expression vector via FX cloning
purNb7	This study. Nanobody candidate VHH#2B-VHH#3E cloned into pSBinit expression vector via FX cloning
purNb8	This study. Nanobody candidate VHH#2B-VHH#12B cloned into pSBinit expression vector via FX cloning

purNb9	This study. Nanobody candidate VHH#3E-VHH#12B cloned into pSBinit expression vector via FX cloning
pSS	This study. Plasmid encoding HlyB and HlyD required for the HlyA secretion system under a constitutive promoter (J23100). Contains chloramphenicol resistance gene.
pNb	This study. Plasmid encoding HlyA and myc-tag under inducible pBad promoter with restriction sites allowing the cloning of the different nanobodies in front of the two tags. Contains ampicillin resistance gene.
pNb1	This study. Nanobody candidate VHH#2B cloned into pNb plasmid via FX cloning
pNb2	This study. Nanobody candidate VHH#3E cloned into into pNb plasmid via FX cloning
pNb3	This study. Nanobody candidate VHH#12B cloned into pNb plasmid via FX cloning
pNb5	This study. Nanobody candidate VHH#3E-VHH#3E cloned into pNb plasmid via FX cloning
pNb7	This study. Nanobody candidate VHH#2B-VHH#3E cloned into pNb plasmid via FX cloning
pNb8	This study. Nanobody candidate VHH#2B-VHH#12B cloned into pSBinit expression vector via FX cloning
pNO1_Nb1	This study. Nanobody candidate VHH#2B cloned into piGEM2.1 plasmid via Gibson
pNO3_Nb1	This study. Nanobody candidate VHH#2B cloned into piGEM2.3 plasmid via Gibson

602

603 **Table 3: Nanobodies used in this study**

Nb ID	Mono or Bivalent	Nb parts	Reference
Nb1	monovalent	VHH#2B	Patent[42]
Nb2	monovalent	VHH#3E	Patent[42]
Nb3	monovalent	VHH#12B	Patent[42]
Nb4	bivalent	VHH#2B	Patent[42]
Nb5	bivalent	VHH#3E	Patent[42]
Nb6	bivalent	VHH#12B	Patent[42]
Nb7	bivalent	VHH#2B+VHH#3E	Patent[42]
Nb8	bivalent	VHH#2B+VHH#12B	Patent[42]
Nb9	bivalent	VHH#3E+VHH#12B	Patent[42]

604

Plate reader fluorescence assay

To measure the activity of all constructs, we transformed plasmids into *E. coli Nissle 1917*. We grew freshly plated single colonies in LB medium supplemented with ampicillin and incubated cultures at 37°C and 220 rpm. On the day of the assay, we spun down the bacteria from the overnight cultures, resuspended them in M9 medium supplemented with ampicillin (M9-Amp) and diluted cultures to OD_{600}=0.5. We then assayed the cultures (20 µL) in a 96-well microplate with 170 µL of M9-Amp and 10 µL of the different compounds tested. We used five different concentrations (8 µM, 31 µM, 125 µM, 500 µM and 2000 µM) of the NO donor diethylenetriamine/nitric oxide (DETA/NO) diluted in ddH2O as the inducer. We quantified cell growth (OD_{600}) and sfGFP fluorescence using a Tecan Spark 10M plate reader. We calculated the responsiveness of the genetic circuit as arbitrary units using the ratio between fluorescence levels and the optical density at 600 nm (reported as sfGFP/OD_{600}) after background correction. As a control for the inducer, we also measured all constructs in the absence of DETA/NO. As a control for cellular autofluorescence background, we also assayed *E. coli Nissle 1917* transformed with the same plasmid but without a promoter to drive sfGFP expression. We measured fluorescence and absorbance at 10-minute intervals for 16 hours at 37 °C and under constant shaking (orbital shaking, 0.1mm orbital averaging). We performed all experiments in technical and biological triplicates. We processed raw data using an ad hoc R script (https://www.r-project.org/).

Flow Cytometry Analysis

We conducted a high-throughput single-cell analysis of bacteria containing variants of the NO detection module and a negative control plasmid (promoterless *sfGFP*) as follows: first, we selected single colonies of the transformed strain (*EcN*) and cultivated them overnight in LB medium supplemented with ampicillin at 37 °C and 220 rpm. Next, we diluted overnight-grown cells in a ratio of 1:10 in fresh LB and grew them overnight at 37 °C and 220 rpm with different

631 concentrations of the DETA/NO inducer (0 mM ,1 mM,1.5 mM, 2 mM). We diluted overnight-
632 grown cells in a ratio of 1:100 in 1mL of filtered cold Dulbecco's PBS (Sigma-Aldrich #D8537)
633 in 15 mL FACS tubes and immediately stored them on ice to halt metabolic processes.
634
635 We set measurements on a BD FACSCantoII machine with the BD FACSDiva 6.1.3 Software
636 after calibration with both CS&T IVD beads and Rainbow Calibration beads (8 peaks, 107/mL,
637 3.0-3.4 µm, RCP-30-5A) for conversion of arbitrary fluorescence units into MEFL. Excitation
638 and emission filters utilized were 488nm and 530/30 nm, respectively. We adjusted side-scatter
639 (SSC) and forward-scatter (FSC) PMT voltages using bacteria from the negative control, until
640 the distribution of each parameter was centered on the scale. We adjusted FITC/GFP PMT
641 voltage using bacteria from the positive control until the upper edge of the "bell curve" from
642 the fluorescent population was one order of magnitude below the upper end of the scale. We
643 acquired a total of 50,000 events for each biological triplicate and washed cells with PBS before
644 measuring when the bacterial density was too high to avoid the formation of aggregates.
645
646 **Nanobodies purification**
647 We transformed *E. coli MC1061* with the pSBinit plasmids containing our 9 different nanobody
648 candidates. The expression vector contains an FX cloning site to insert our different nanobody
649 fragments ordered. The C-terminal myc and 6xHis-tags are included on the plasmid backbone
650 and automatically added in case of a successful FX cloning (Figure 2a). We grew the cells in
651 600 ml liquid cultures (1:1000 dilution of antibiotic) at 37°C until an OD of 0.4 to 0.7 was
652 reached. We then induced the expression by the addition of 0.02% L-arabinose and allowed
653 bacteria to express the nanobodies for 16 hours at 22°C. We spun down cells at 4'500 rpm for
654 15 min at 4°C and transferred the resulting supernatant to a bottle with 20 nM imidazole pH
655 7.5. To extract the nanobodies from the solution, we performed a batch binding using 5 ml Ni-
656 NTA resin for 2 hours while shaking. We poured the resin into gravity flow columns and washed

657 them with TBS pH 7.5, 30 mM imidazole. We eluted nanobodies with 10 ml TBS pH 7.5 and
658 30 mM imidazole and collected them into fractions, which we measured with the NanoDrop
659 spectrophotometer (Thermo Fisher Scientific). We pooled the fractions with low concentrations
660 and further concentrated them using concentration columns (spun at 2'500 g in 10 kDa
661 concentrators). Lastly, we loaded the purified nanobody candidates on the Sepax in TBS (pH
662 7.5).
663
664 **Cultivation of THP-1 non-adherent human monocytes**
665 We substituted growth medium (RPMI 1640, Gibco) with 10% fetal bovine serum (FBS) and
666 stored at 4°C. We maintained cell densities between 0.1 and 1.0 x 10^6 cells/ml, splitting them
667 at a ratio of 1:2 or 1:3 (approximately 0.5 x 10^6 cells/ml) every 3 to 4 days. THP-1 cells display
668 a doubling time of roughly 35 -50 hours. During splitting, we transferred cells into 50ml falcon
669 tubes and centrifuged them at 1700 rpm for 5 minutes. We removed the supernatant and
670 resuspended cells in fresh media. After counting the cells, we seeded them at the optimal density.
671
672 **Cell Assay**
673 Before the beginning of the actual cell assay, we centrifuged THP-1 cells and resuspended them
674 in starvation media (RPMI 1640 without FBS) and seeded at a density of 1 *x* 10^6 cells / ml in a
675 96-well plate (final volume: 200 µl). We then incubated cells for 24 hours at 37°C with 5%
676 CO2, according to the cell specific cultivation protocol.
677
678 The next day, we prepared a TNFα dilution series (100 ng/ml, 50 ng/ml, 10 ng/ml, 5 ng/ml, 1
679 ng/ml, 0.5 ng/ml, 0.1 ng/ml) and kept them on ice. Additionally, we diluted the nanobodies to
680 a final concentration of approximately 100 nM and stored them on ice. After starving the cells
681 for 24 hours, we added the diluted nanobodies to the well plate and gently shook the plate before
682 incubating it for 30 minutes. Afterwards, we stimulated the cells with rTNFα and incubated

683 them for 24 hours at 37°C with 5% CO2. We then harvested the cells, transferred them to
684 Eppendorf tubes, and centrifuged them at 3.5g for 10 minutes at 4°C. After removing the
685 supernatant, we froze the cell pellet with liquid nitrogen and stored it at -80°C for further
686 quantitative RT-qPCR analysis.
687
688 **Induction of Nanobody Production and Secretion**
689 We inoculated successfully double-transformed bacteria in 5 ml precultures with a 1:1000
690 antibiotic dilution and incubated them at 37°C overnight while shaking at 120 r.p.m. The next
691 day, we transferred the cells to 10 ml TB with a 1:1000 antibiotic dilution and grew them at
692 37°C while shaking until an OD600 of approximately 0.6 was reached. To induce secretion, we
693 added either L-arabinose (final concentration: 0.02%) or diethylenetriamine/nitric oxide
694 (DETA/NO) (testing different concentrations), depending on the transformed cells and their
695 nanobody plasmid. We incubated the cultures at 37°C overnight to allow them to express and
696 secrete nanobodies. We then spun down the cells and collected 2 ml of supernatant for testing
697 via Western Blot or ELISA.
698
699 If we needed to test the cell lysate, we first resuspended the cells in TBS and transferred them
700 to a screw-lid microcentrifuge tube. We added one PCR tube of glass beads and lysed the cells
701 using the maxiprep machine at 4 m/s for 20 seconds. We placed the cells on ice for 5 minutes
702 for recovery. We then repeated the shaking process twice, with 5-minute rest intervals in
703 between.
704
705 **ELISA**
706 The night before the experiment, we coated a 96-well Nunc Maxicrop immunoplate with 100
707 µl of protein A solution (1:1000 dilution in PBS) in each well, sealed the plate, and incubated
708 it at 4°C overnight. Before starting the experiment, we freshly prepared the buffers according

to the following specifications for ELISA: Tris-buffered saline (TBS) at 1x concentration; TBS-BSA, which is TBS supplemented with 0.5% Bovine Serum Albumin (BSA, weight/volume); TBS-D, consisting of TBS supplemented with a detergent of choice at an amount equivalent to three times the Critical Micelle Concentration (CMC) of the chosen detergent; and TBS-BSA-D, combining TBS with both 0.5% BSA and 0.1% of the chosen detergent (weight/volume). We washed each well with 250 µl TBS and then blocked them with 250 µl TBS-BSA for 30 minutes. We washed the plate three times with 250 µl TBS per well. Then, we added 100 µl of 1:2000 diluted monoclonal anti-c-myc antibody (diluted in TBS-BSA-D) to each well and incubated for 20 minutes. We washed the plate three times with 250 µl TBS-D and added samples diluted in TBS-BSA-D (20 µl in 80 µl solvent for supernatant or periplasmic extraction, or approximately 50 nM for purified nanobodies). We washed the plate three times with 250 µl TBS-D, then added 100 µl of 50 nM biotinylated TNFα in TBS-BSA-D and incubated for 20 minutes. We washed the plate three times with 250 µl TBS-D before adding 100 µl of 1:5000 diluted streptavidin-peroxidase polymer solutions (diluted in TBS-BSA-D) and incubating for 20 minutes. After washing the plate three times with 250 µl TBS-D, we added 100 µl of ELISA developing buffer and incubated until individual wells turned blue, which took between 5 to 15 minutes. We then measured the absorbance at 650 nm using a plate reader. ELISA signals as small as 1.5-fold above the background can indicate a high-affinity binder.

ASSOCIATED CONTENT

Supplementary Information is linked to the online version of the paper

Acknowledgements:
We extend our gratitude to the UZurich 2022 iGEM team for their collective efforts in developing this study. Special thanks to Timothy Kurrer for his support throughout the competition, and to Yen Way Isabell Trinh and Christian Andres Ramos Uria for their insights on our mathematical model. We also thank the UZH flow cytometry facility for their technical support and the gastroenterologists from IBD Net for their feedback. Lastly, we appreciate Professors Markus Seeger from UZH for welcoming us in his group, and Richard Murray from Caltech for sharing his expertise and protocols related to *Escherichia coli Nissle*.

Author contributions: All authors conceived the study and designed experiments.
L.B, J.M., **M.M.**, **K.J.** and **C.A.W.** carried out NO-induced fluorescent reporter assays, analyzed data, and generated figures.
G.A., **N.W.**, **F.A.** and **J.E.** carried out nanobody production, purification and activity assays, analyzed data, and generated figures.
G.A., **N.W.**, **F.A.** and **J.E.** carried out NO-induced anti-TNF nanobodies secretion assays, analyzed data, and generated figures.
A.M. and **A.S** carried out modelling, simulations, and generated figures.
N. W., **M. C.**, **A. S.**, **G. A.** and **M. M.**, contributed with the writing and editing of the paper.
C.A.W. wrote the final version of the paper.

Data availability: The data generated in this study will be deposited in a public repository upon manuscript acceptance.

Computer code: The computer code will be shared in a public repository upon manuscript acceptance.

Competing interests: The authors declare no competing interest.

Corresponding authors: Correspondence to caua.westmann@ieu.uzh.ch

Supporting Information: The general methods employed in this study include PCR (Section 1.1), real-time quantitative PCR (Section 1.2), preparation of calcium-competent EcN (Section 1.3), heat-shock transformation of calcium-competent EcN (Section 1.4), Gibson assembly (Section 1.5), preparation of electrocompetent EcN (Section 1.6), electroporation (Section 1.7), and Western Blot (Section 1.8). The plasmid design and construction cover secretion plasmid design (Section 2.1), NO-sensing plasmid design (Section 2.2), and plasmid cloning (Section 2.3). Model supplementary methods include assumptions and parameters (Section 3.1), number of inflammatory sites (Section 3.2), number of bacteria (Section 3.3), emission coefficients (Section 3.4), diffusion coefficients (Section 3.5), emission dynamics (Section 3.6), and diffusion dynamics (Section 3.7). Supplementary tables list oligonucleotides used (Table S1). Supplementary figures feature the plasmid map of the negative control (Figure S1), the plasmid map of the engineered nitric oxide sensor construct piGEM2 (ß-1) (Figure S2), the plasmid map of the engineered nitric oxide sensor construct piGEM3 (WT) (Figure S3), the effect of DETA/NO on cellular growth (Figure S4), the impact of removing the plasmid-expressed NorR on NO sensitivity and response strength (Figure S5), the plasmid map of the nanobody purification plasmid (Figure S6), the plasmid map of the arabinose-induced nanobody expression plasmid (Figure S7), the plasmid map of the secretion system plasmid (Figure S8),

778 the plasmid map of the NO-induced nanobody expression plasmid (ß-2) (Figure S9), the
779 purification of monovalent and bivalent anti-TNFα nanobodies from E. coli MC1061 (Figure
780 S10), the comparison of over day to overnight arabinose-induced nanobody secretion in E. coli
781 MC1061 (Figure S11), the arabinose-induced anti-TNFα nanobody production in E. coli
782 MC1061 (Figure S12), the arabinose-induced anti-TNFα nanobody production in E. coli Nissle
783 1917 (Figure S13), the analysis of ELISA comparing the binding capabilities of purified and
784 secreted monovalent and bivalent anti-TNFα nanobodies in E. coli Nissle 1917 and E. coli
785 MC1061 (Figure S14), the NO-induced monovalent anti-TNFα nanobody expression in E. coli
786 Nissle 1917 (Figure S15), and a visual comparison between diffusion models (Figure S16).
787 (PDF).

788 **Funding:** This study was supported by multiple funding sources. Academic funding was
789 provided by the University of Zurich through the UZH Alumni Science, the Faculty of Science
790 (MNF), the Faculty of Medicine, the Vice President Research, and the President's Services.
791 Private sponsorship was provided by Pierre Fabre, Microsynth, the Swiss Academy of Sciences
792 (SCNAT), and Promega. Additionally, this publication was funded by the University of Zurich
793 and the Consortium of Swiss Academic Libraries, making it available as open access.

794

795 **REFERENCES**

796

797 (1) Szigethy, E.; McLafferty, L.; Goyal, A. Inflammatory Bowel Disease. *Child Adolesc*
798 *Psychiatr Clin N Am* **2010**, *19* (2), 301–318. https://doi.org/10.1016/j.chc.2010.01.007.
799 (2) Guan, Q. A Comprehensive Review and Update on the Pathogenesis of Inflammatory
800 Bowel Disease. *J Immunol Res* **2019**, *2019*, 1–16. https://doi.org/10.1155/2019/7247238.
801 (3) Ng, S. C.; Shi, H. Y.; Hamidi, N.; Underwood, F. E.; Tang, W.; Benchimol, E. I.;
802 Panaccione, R.; Ghosh, S.; Wu, J. C. Y.; Chan, F. K. L.; Sung, J. J. Y.; Kaplan, G. G.
803 Worldwide Incidence and Prevalence of Inflammatory Bowel Disease in the 21st
804 Century: A Systematic Review of Population-Based Studies. *The Lancet* **2017**, *390*
805 (10114), 2769–2778. https://doi.org/10.1016/S0140-6736(17)32448-0.
806 (4) Alatab, S.; Sepanlou, S. G.; Ikuta, K.; Vahedi, H.; Bisignano, C.; Safiri, S.; Sadeghi, A.;
807 Nixon, M. R.; Abdoli, A.; Abolhassani, H.; Alipour, V.; Almadi, M. A. H.; Almasi-
808 Hashiani, A.; Anushiravani, A.; Arabloo, J.; Atique, S.; Awasthi, A.; Badawi, A.; Baig, A.
809 A. A.; Bhala, N.; Bijani, A.; Biondi, A.; Borzì, A. M.; Burke, K. E.; Carvalho, F.; Daryani,
810 A.; Dubey, M.; Eftekhari, A.; Fernandes, E.; Fernandes, J. C.; Fischer, F.; Haj-Mirzaian,
811 A.; Haj-Mirzaian, A.; Hasanzadeh, A.; Hashemian, M.; Hay, S. I.; Hoang, C. L.; Househ,
812 M.; Ilesanmi, O. S.; Jafari Balalami, N.; James, S. L.; Kengne, A. P.; Malekzadeh, M.
813 M.; Merat, S.; Meretoja, T. J.; Mestrovic, T.; Mirrakhimov, E. M.; Mirzaei, H.;
814 Mohammad, K. A.; Mokdad, A. H.; Monasta, L.; Negoi, I.; Nguyen, T. H.; Nguyen, C.
815 T.; Pourshams, A.; Poustchi, H.; Rabiee, M.; Rabiee, N.; Ramezanzadeh, K.; Rawaf, D.
816 L.; Rawaf, S.; Rezaei, N.; Robinson, S. R.; Ronfani, L.; Saxena, S.; Sepehrimanesh, M.;
817 Shaikh, M. A.; Sharafi, Z.; Sharif, M.; Siabani, S.; Sima, A. R.; Singh, J. A.; Soheili, A.;
818 Sotoudehmanesh, R.; Suleria, H. A. R.; Tesfay, B. E.; Tran, B.; Tsoi, D.; Vacante, M.;
819 Wondmieneh, A. B.; Zarghi, A.; Zhang, Z.-J.; Dirac, M.; Malekzadeh, R.; Naghavi, M.
820 The Global, Regional, and National Burden of Inflammatory Bowel Disease in 195
821 Countries and Territories, 1990–2017: A Systematic Analysis for the Global Burden of
822 Disease Study 2017. *Lancet Gastroenterol Hepatol* **2020**, *5* (1), 17–30.
823 https://doi.org/10.1016/S2468-1253(19)30333-4.
824 (5) Zhang, Y.-Z. Inflammatory Bowel Disease: Pathogenesis. *World J Gastroenterol* **2014**,
825 *20* (1), 91. https://doi.org/10.3748/wjg.v20.i1.91.
826 (6) Cai, Z.; Wang, S.; Li, J. Treatment of Inflammatory Bowel Disease: A Comprehensive
827 Review. *Front Med (Lausanne)* **2021**, *8*. https://doi.org/10.3389/fmed.2021.765474.
828 (7) Genaro, L. M.; Gomes, L. E. M.; Franceschini, A. P. M. de F.; Ceccato, H. D.; de Jesus,
829 R. N.; Lima, A. P.; Nagasako, C. K.; Fagundes, J. J.; Ayrizono, M. de L. S.; Leal, R. F.
830 Anti-TNF Therapy and Immunogenicity in Inflammatory Bowel Diseases: A
831 Translational Approach. *Am J Transl Res* **2021**, *13* (12), 13916–13930.
832 (8) Sands, B. E.; Kaplan, G. G. The Role of TNFα in Ulcerative Colitis. *The Journal of*
833 *Clinical Pharmacology* **2007**, *47* (8), 930–941.
834 https://doi.org/10.1177/0091270007301623.
835 (9) Rutgeerts, P.; Sandborn, W. J.; Feagan, B. G.; Reinisch, W.; Olson, A.; Johanns, J.;
836 Travers, S.; Rachmilewitz, D.; Hanauer, S. B.; Lichtenstein, G. R.; de Villiers, W. J. S.;
837 Present, D.; Sands, B. E.; Colombel, J. F. Infliximab for Induction and Maintenance
838 Therapy for Ulcerative Colitis. *New England Journal of Medicine* **2005**, *353* (23), 2462–
839 2476. https://doi.org/10.1056/NEJMoa050516.
840 (10) Windsor, J. W.; Kaplan, G. G. Evolving Epidemiology of IBD. *Curr Gastroenterol Rep*
841 **2019**, *21* (8), 40. https://doi.org/10.1007/s11894-019-0705-6.
842 (11) Elhag, D. A.; Kumar, M.; Saadaoui, M.; Akobeng, A. K.; Al-Mudahka, F.; Elawad, M.;
843 Al Khodor, S. Inflammatory Bowel Disease Treatments and Predictive Biomarkers of

Therapeutic Response. *Int J Mol Sci* **2022**, *23* (13), 6966. https://doi.org/10.3390/ijms23136966.

(12) Pedrolli, D. B.; Ribeiro, N. V.; Squizato, P. N.; de Jesus, V. N.; Cozetto, D. A. Engineering Microbial Living Therapeutics: The Synthetic Biology Toolbox. *Trends Biotechnol* **2018**, *0* (0). https://doi.org/10.1016/j.tibtech.2018.09.005.

(13) Cubillos-Ruiz, A.; Guo, T.; Sokolovska, A.; Miller, P. F.; Collins, J. J.; Lu, T. K.; Lora, J. M. Engineering Living Therapeutics with Synthetic Biology. *Nat Rev Drug Discov* **2021**, *20* (12), 941–960. https://doi.org/10.1038/s41573-021-00285-3.

(14) Shan, Y.; Lee, M.; Chang, E. B. The Gut Microbiome and Inflammatory Bowel Diseases. *Annu Rev Med* **2022**, *73* (1), 455–468. https://doi.org/10.1146/annurev-med-042320-021020.

(15) Nissle, A. Weiteres Über Grundlagen Und Praxis Der Mutaflorbehandlung. *DMW-Deutsche Medizinische Wochenschrift* **1925**, *51* (44), 1809–1813.

(16) Nissle, A. Die Antagonistische Behandlung Chronischer Darmstörungen Mit Colibakterien. *Med Klin* **1918**, *2*, 29–33.

(17) Sonnenborn, U.; Schulze, J. The Non-Pathogenic *Escherichia Coli* Strain Nissle 1917 – Features of a Versatile Probiotic. *Microb Ecol Health Dis* **2009**, *21* (3–4), 122–158. https://doi.org/10.3109/08910600903444267.

(18) Torres, J.; [ECCO], on behalf of the E. C. and C. O.; Bonovas, S.; [ECCO], on behalf of the E. C. and C. O.; Doherty, G.; [ECCO], on behalf of the E. C. and C. O.; Kucharzik, T.; [ECCO], on behalf of the E. C. and C. O.; Gisbert, J. P.; [ECCO], on behalf of the E. C. and C. O.; Raine, T.; [ECCO], on behalf of the E. C. and C. O.; Adamina, M.; [ECCO], on behalf of the E. C. and C. O.; Armuzzi, A.; [ECCO], on behalf of the E. C. and C. O.; Bachmann, O.; [ECCO], on behalf of the E. C. and C. O.; Bager, P.; [ECCO], on behalf of the E. C. and C. O.; Biancone, L.; [ECCO], on behalf of the E. C. and C. O.; Bokemeyer, B.; [ECCO], on behalf of the E. C. and C. O.; Bossuyt, P.; [ECCO], on behalf of the E. C. and C. O.; Burisch, J.; [ECCO], on behalf of the E. C. and C. O.; Collins, P.; [ECCO], on behalf of the E. C. and C. O.; El-Hussuna, A.; [ECCO], on behalf of the E. C. and C. O.; Ellul, P.; [ECCO], on behalf of the E. C. and C. O.; Frei-Lanter, C.; [ECCO], on behalf of the E. C. and C. O.; Furfaro, F.; [ECCO], on behalf of the E. C. and C. O.; Gingert, C.; [ECCO], on behalf of the E. C. and C. O.; Gionchetti, P.; [ECCO], on behalf of the E. C. and C. O.; Gomollon, F.; [ECCO], on behalf of the E. C. and C. O.; González-Lorenzo, M.; [ECCO], on behalf of the E. C. and C. O.; Gordon, H.; [ECCO], on behalf of the E. C. and C. O.; Hlavaty, T.; [ECCO], on behalf of the E. C. and C. O.; Juillerat, P.; [ECCO], on behalf of the E. C. and C. O.; Katsanos, K.; [ECCO], on behalf of the E. C. and C. O.; Kopylov, U.; [ECCO], on behalf of the E. C. and C. O.; Krustins, E.; [ECCO], on behalf of the E. C. and C. O.; Lytras, T.; [ECCO], on behalf of the E. C. and C. O.; Maaser, C.; [ECCO], on behalf of the E. C. and C. O.; Magro, F.; [ECCO], on behalf of the E. C. and C. O.; Kenneth Marshall, J.; [ECCO], on behalf of the E. C. and C. O.; Myrelid, P.; [ECCO], on behalf of the E. C. and C. O.; Pellino, G.; [ECCO], on behalf of the E. C. and C. O.; Rosa, I.; [ECCO], on behalf of the E. C. and C. O.; Sabino, J.; [ECCO], on behalf of the E. C. and C. O.; Savarino, E.; [ECCO], on behalf of the E. C. and C. O.; Spinelli, A.; [ECCO], on behalf of the E. C. and C. O.; Stassen, L.; [ECCO], on behalf of the E. C. and C. O.; Uzzan, M.; [ECCO], on behalf of the E. C. and C. O.; Vavricka, S.; [ECCO], on behalf of the E. C. and C. O.; Verstockt, B.; [ECCO], on behalf of the E. C. and C. O.; Warusavitarne, J.; [ECCO], on behalf of the E. C. and C. O.; Zmora, O.; [ECCO], on behalf of the E. C. and C. O.; Fiorino, G.; [ECCO], on behalf of the E. C. and C. O. ECCO Guidelines on Therapeutics in Crohn's Disease: Medical Treatment. *J Crohns Colitis* **2020**, *14* (1), 4–22. https://doi.org/10.1093/ECCO-JCC/JJZ180.

(19) Raine, T.; Bonovas, S.; Burisch, J.; Kucharzik, T.; Adamina, M.; Annese, V.; Bachmann, O.; Bettenworth, D.; Chaparro, M.; Czuber-Dochan, W.; Eder, P.; Ellul, P.; Fidalgo, C.; Fiorino, G.; Gionchetti, P.; Gisbert, J. P.; Gordon, H.; Hedin, C.; Holubar, S.; Iacucci, M.; Karmiris, K.; Katsanos, K.; Kopylov, U.; Lakatos, P. L.; Lytras, T.; Lyutakov, I.; Noor, N.; Pellino, G.; Piovani, D.; Savarino, E.; Selvaggi, F.; Verstockt, B.; Spinelli, A.; Panis, Y.; Doherty, G. ECCO Guidelines on Therapeutics in Ulcerative Colitis: Medical Treatment. *J Crohns Colitis* **2022**, *16* (1), 2–17. https://doi.org/10.1093/ECCO-JCC/JJAB178.

(20) Gordon, H.; Biancone, L.; Fiorino, G.; Katsanos, K. H.; Kopylov, U.; Al Sulais, E.; Axelrad, J. E.; Balendran, K.; Burisch, J.; De Ridder, L.; Derikx, L.; Ellul, P.; Greuter, T.; Iacucci, M.; Di Jiang, C.; Kapizioni, C.; Karmiris, K.; Kirchgesner, J.; Laharie, D.; Lobatón, T.; Molnár, T.; Noor, N. M.; Rao, R.; Saibeni, S.; Scharl, M.; Vavricka, S. R.; Raine, T. ECCO Guidelines on Inflammatory Bowel Disease and Malignancies. *J Crohns Colitis* **2023**, *17* (6), 827–854. https://doi.org/10.1093/ECCO-JCC/JJAC187.

(21) Schultz, M. Clinical Use of E. Coli Nissle 1917 in Inflammatory Bowel Disease. *Inflamm Bowel Dis* **2008**, *14* (7), 1012–1018. https://doi.org/10.1002/ibd.20377.

(22) Ukena, S. N.; Singh, A.; Dringenberg, U.; Engelhardt, R.; Seidler, U.; Hansen, W.; Bleich, A.; Bruder, D.; Franzke, A.; Rogler, G.; Suerbaum, S.; Buer, J.; Gunzer, F.; Westendorf, A. M. Probiotic Escherichia Coli Nissle 1917 Inhibits Leaky Gut by Enhancing Mucosal Integrity. *PLoS One* **2007**, *2* (12), e1308. https://doi.org/10.1371/journal.pone.0001308.

(23) Matthes, H.; Krummenerl, T.; Giensch, M.; Wolff, C.; Schulze, J. Clinical Trial: Probiotic Treatment of Acute Distal Ulcerative Colitis with Rectally Administered Escherichia Coli Nissle 1917 (EcN). *BMC Complement Altern Med* **2010**, *10* (1), 13. https://doi.org/10.1186/1472-6882-10-13.

(24) Kruis, W. Maintaining Remission of Ulcerative Colitis with the Probiotic Escherichia Coli Nissle 1917 Is as Effective as with Standard Mesalazine. *Gut* **2004**, *53* (11), 1617–1623. https://doi.org/10.1136/gut.2003.037747.

(25) Dong, Y.; Xu, T.; Xiao, G.; Hu, Z.; Chen, J. Opportunities and Challenges for Synthetic Biology in the Therapy of Inflammatory Bowel Disease. *Front Bioeng Biotechnol* **2022**, *10*. https://doi.org/10.3389/fbioe.2022.909591.

(26) Lynch, J. P.; Goers, L.; Lesser, C. F. Emerging Strategies for Engineering Escherichia Coli Nissle 1917-Based Therapeutics. *Trends Pharmacol Sci* **2022**, *43* (9), 772–786. https://doi.org/10.1016/j.tips.2022.02.002.

(27) Ba, F.; Zhang, Y.; Ji, X.; Liu, W.; Ling, S.; Li, J. Expanding the Toolbox of Probiotic *Escherichia Coli* Nissle 1917 for Synthetic Biology. *Biotechnol J* **2023**. https://doi.org/10.1002/biot.202300327.

(28) Kurtz, C. B.; Millet, Y. A.; Puurunen, M. K.; Perreault, M.; Charbonneau, M. R.; Isabella, V. M.; Kotula, J. W.; Antipov, E.; Dagon, Y.; Denney, W. S.; Wagner, D. A.; West, K. A.; Degar, A. J.; Brennan, A. M.; Miller, P. F. An Engineered *E. Coli* Nissle Improves Hyperammonemia and Survival in Mice and Shows Dose-Dependent Exposure in Healthy Humans. *Sci Transl Med* **2019**, *11* (475). https://doi.org/10.1126/scitranslmed.aau7975.

(29) Isabella, V. M.; Ha, B. N.; Castillo, M. J.; Lubkowicz, D. J.; Rowe, S. E.; Millet, Y. A.; Anderson, C. L.; Li, N.; Fisher, A. B.; West, K. A.; Reeder, P. J.; Momin, M. M.; Bergeron, C. G.; Guilmain, S. E.; Miller, P. F.; Kurtz, C. B.; Falb, D. Development of a Synthetic Live Bacterial Therapeutic for the Human Metabolic Disease Phenylketonuria. *Nat Biotechnol* **2018**, *36* (9), 857–864. https://doi.org/10.1038/nbt.4222.

(30) Praveschotinunt, P.; Duraj-Thatte, A. M.; Gelfat, I.; Bahl, F.; Chou, D. B.; Joshi, N. S. Engineered E. Coli Nissle 1917 for the Delivery of Matrix-Tethered Therapeutic Domains to the Gut. *Nat Commun* **2019**, *10* (1), 5580. https://doi.org/10.1038/s41467-019-13336-6.

(31) Gelfat, I.; Aqeel, Y.; Tremblay, J. M.; Jaskiewicz, J. J.; Shrestha, A.; Lee, J. N.; Hu, S.; Qian, X.; Magoun, L.; Sheoran, A.; Bedenice, D.; Giem, C.; Manjula-Basavanna, A.; Pulsifer, A. R.; Tu, H. X.; Li, X.; Minus, M. L.; Osburne, M. S.; Tzipori, S.; Shoemaker, C. B.; Leong, J. M.; Joshi, N. S. Single Domain Antibodies against Enteric Pathogen Virulence Factors Are Active as Curli Fiber Fusions on Probiotic E. Coli Nissle 1917. *PLoS Pathog* **2022**, *18* (9). https://doi.org/10.1371/JOURNAL.PPAT.1010713.

(32) Zou, Z. P.; Du, Y.; Fang, T. T.; Zhou, Y.; Ye, B. C. Biomarker-Responsive Engineered Probiotic Diagnoses, Records, and Ameliorates Inflammatory Bowel Disease in Mice. *Cell Host Microbe* **2023**, *31* (2), 199-212.e5. https://doi.org/10.1016/J.CHOM.2022.12.004.

(33) Lynch, J. P.; González-Prieto, C.; Reeves, A. Z.; Bae, S.; Powale, U.; Godbole, N. P.; Tremblay, J. M.; Schmidt, F. I.; Ploegh, H. L.; Kansra, V.; Glickman, J. N.; Leong, J. M.; Shoemaker, C. B.; Garrett, W. S.; Lesser, C. F. Engineered Escherichia Coli for the in Situ Secretion of Therapeutic Nanobodies in the Gut. *Cell Host Microbe* **2023**, *31* (4), 634-649.e8. https://doi.org/10.1016/j.chom.2023.03.007.

(34) Liu, Y.; Zhu, Z.; Jiang, L. Programming Therapeutic Probiotics by Self-Tunable Sense-and-Respond Genetic Circuits. *Trends Microbiol* **2023**, *31* (11), 1099–1101. https://doi.org/10.1016/j.tim.2023.08.001.

(35) Soufli, I.; Toumi, R.; Rafa, H.; Touil-Boukoffa, C. Overview of Cytokines and Nitric Oxide Involvement in Immuno-Pathogenesis of Inflammatory Bowel Diseases. *World J Gastrointest Pharmacol Ther* **2016**, *7* (3), 353. https://doi.org/10.4292/wjgpt.v7.i3.353.

(36) Avdagić, N.; Zaćiragić, A.; Babić, N.; Hukić, M.; Šeremet, M.; Lepara, O.; Nakaš-Ićindić, E. Nitric Oxide as a Potential Biomarker in Inflammatory Bowel Disease. *Bosn J Basic Med Sci* **2013**, *13* (1), 5. https://doi.org/10.17305/bjbms.2013.2402.

(37) Schairer, D. O.; Chouake, J. S.; Nosanchuk, J. D.; Friedman, A. J. The Potential of Nitric Oxide Releasing Therapies as Antimicrobial Agents. *Virulence* **2012**, *3* (3), 271–279. https://doi.org/10.4161/viru.20328.

(38) Chen, X. J.; Wang, B.; Thompson, I. P.; Huang, W. E. Rational Design and Characterization of Nitric Oxide Biosensors in *E. Coli* Nissle 1917 and Mini SimCells. *ACS Synth Biol* **2021**, *10* (10), 2566–2578. https://doi.org/10.1021/acssynbio.1c00223.

(39) Muyldermans, S. Nanobodies: Natural Single-Domain Antibodies. *Annu Rev Biochem* **2013**, *82*, 775–797. https://doi.org/10.1146/ANNUREV-BIOCHEM-063011-092449.

(40) Hamers-Casterman, C.; Atarhouch, T.; Muyldermans, S.; Robinson, G.; Hammers, C.; Songa, E. B.; Bendahman, N.; Hammers, R. Naturally Occurring Antibodies Devoid of Light Chains. *Nature 1993 363:6428* **1993**, *363* (6428), 446–448. https://doi.org/10.1038/363446a0.

(41) Vincke, C.; Loris, R.; Saerens, D.; Martinez-Rodriguez, S.; Muyldermans, S.; Conrath, K. General Strategy to Humanize a Camelid Single-Domain Antibody and Identification of a Universal Humanized Nanobody Scaffold. *Journal of Biological Chemistry* **2009**, *284* (5), 3273–3284. https://doi.org/10.1074/jbc.M806889200.

(42) Silence, K.; Lauwereys, M.; De Haard, H. Single Domain Antibodies Directed against Tumour Necrosis Factor-Alpha and Uses Therefor. US20090022721A1, 2003.

(43) Dalbey, R. E.; Kuhn, A. Protein Traffic in Gram-Negative Bacteria – How Exported and Secreted Proteins Find Their Way. *FEMS Microbiol Rev* **2012**, *36* (6), 1023–1045. https://doi.org/10.1111/J.1574-6976.2012.00327.X.

(44) Holland, I. B.; Kenny, B.; Blight, M. Haemolysin Secretion from E Coli. *Biochimie* **1990**, *72* (2–3), 131–141. https://doi.org/10.1016/0300-9084(90)90138-7.

(45) Blight, M. A.; Chervaux, C.; Holland, I. B. Protein Secretion Pathways in Escherichia Coli. *Curr Opin Biotechnol* **1994**, *5* (5), 468–474. https://doi.org/10.1016/0958-1669(94)90059-0.

(46) Green, E. R.; Mecsas, J. Bacterial Secretion Systems: An Overview. *Microbiol Spectr* **2016**, *4* (1). https://doi.org/10.1128/microbiolspec.VMBF-0012-2015.

(47) Fraile, S.; Muñoz, A.; De Lorenzo, V.; Fernández, L. A. Secretion of Proteins with Dimerization Capacity by the Haemolysin Type I Transport System of *Escherichia Coli*. *Mol Microbiol* **2004**, *53* (4), 1109–1121. https://doi.org/10.1111/j.1365-2958.2004.04205.x.

(48) Ruano-Gallego, D.; Fraile, S.; Gutierrez, C.; Fernández, L. Á. Screening and Purification of Nanobodies from E. Coli Culture Supernatants Using the Hemolysin Secretion System. *Microb Cell Fact* **2019**, *18* (1), 47. https://doi.org/10.1186/s12934-019-1094-0.

(49) Hutchings, M. I.; Mandhana, N.; Spiro, S. The NorR Protein of *Escherichia Coli* Activates Expression of the Flavorubredoxin Gene *NorV* in Response to Reactive Nitrogen Species. *J Bacteriol* **2002**, *184* (16), 4640–4643. https://doi.org/10.1128/JB.184.16.4640-4643.2002.

(50) Gardner, A. M.; Gessner, C. R.; Gardner, P. R. Regulation of the Nitric Oxide Reduction Operon (NorRVW) in Escherichia Coli. *Journal of Biological Chemistry* **2003**, *278* (12), 10081–10086. https://doi.org/10.1074/jbc.M212462200.

(51) D'Autréaux, B.; Tucker, N. P.; Dixon, R.; Spiro, S. A Non-Haem Iron Centre in the Transcription Factor NorR Senses Nitric Oxide. *Nature* **2005**, *437* (7059), 769–772. https://doi.org/10.1038/nature03953.

(52) Tucker, N. P.; D'Autréaux, B.; Spiro, S.; Dixon, R. Mechanism of Transcriptional Regulation by the *Escherichia Coli* Nitric Oxide Sensor NorR. *Biochem Soc Trans* **2006**, *34* (1), 191–194. https://doi.org/10.1042/BST0340191.

(53) Pédelacq, J. D.; Cabantous, S.; Tran, T.; Terwilliger, T. C.; Waldo, G. S. Engineering and Characterization of a Superfolder Green Fluorescent Protein. *Nat Biotechnol* **2006**, *24* (1), 79–88. https://doi.org/10.1038/nbt1172.

(54) Mancinelli, R. L.; McKay, C. P. Effects of Nitric Oxide and Nitrogen Dioxide on Bacterial Growth. *Appl Environ Microbiol* **1983**, *46* (1), 198–202. https://doi.org/10.1128/AEM.46.1.198-202.1983.

(55) Korostelev, A. A. The Structural Dynamics of Translation. *Annu Rev Biochem* **2022**, *91* (Volume 91, 2022), 245–267. https://doi.org/10.1146/ANNUREV-BIOCHEM-071921-122857/CITE/REFWORKS.

(56) Gingold, H.; Pilpel, Y. Determinants of Translation Efficiency and Accuracy. *Mol Syst Biol* **2011**, *7*. https://doi.org/10.1038/MSB.2011.14.

(57) Unoson, C.; Gerhart, E.; Wagner, H.; Gerhart, / E. Dealing with Stable Structures at Ribosome Binding Sites: Bacterial Translation and Ribosome Standby. *RNA Biol* **2007**, *4* (3), 113–117. https://doi.org/10.4161/RNA.4.3.5350.

(58) Zimmermann, I.; Egloff, P.; Hutter, C. A.; Arnold, F. M.; Stohler, P.; Bocquet, N.; Hug, M. N.; Huber, S.; Siegrist, M.; Hetemann, L.; Gera, J.; Gmür, S.; Spies, P.; Gygax, D.; Geertsma, E. R.; Dawson, R. J.; Seeger, M. A. Synthetic Single Domain Antibodies for the Conformational Trapping of Membrane Proteins. *Elife* **2018**, *7*. https://doi.org/10.7554/eLife.34317.

(59) Lee, S. H.; Kwon, J. eun; Cho, M.-L. Immunological Pathogenesis of Inflammatory Bowel Disease. *Intest Res* **2018**, *16* (1), 26. https://doi.org/10.5217/ir.2018.16.1.26.

(60) Scheinfeld, N. Adalimumab (HUMIRA): A Review. *J Drugs Dermatol* **2003**, *2* (4), 375–377.

(61) Schöneberg, J.; Ullrich, A.; Noé, F. Simulation Tools for Particle-Based Reaction-Diffusion Dynamics in Continuous Space. *BMC Biophys* **2014**, *7* (1), 11. https://doi.org/10.1186/s13628-014-0011-5.

(62) Andrews, S. S.; Bray, D. Stochastic Simulation of Chemical Reactions with Spatial Resolution and Single Molecule Detail. *Phys Biol* **2004**, *1* (3), 137–151. https://doi.org/10.1088/1478-3967/1/3/001.

(63) Chew, W.-X.; Kaizu, K.; Watabe, M.; Muniandy, S. V.; Takahashi, K.; Arjunan, S. N. V. Surface Reaction-Diffusion Kinetics on Lattice at the Microscopic Scale. *Phys Rev E* **2019**, *99* (4), 042411. https://doi.org/10.1103/PhysRevE.99.042411.

(64) Kerr, R. A.; Bartol, T. M.; Kaminsky, B.; Dittrich, M.; Chang, J.-C. J.; Baden, S. B.; Sejnowski, T. J.; Stiles, J. R. Fast Monte Carlo Simulation Methods for Biological Reaction-Diffusion Systems in Solution and on Surfaces. *SIAM Journal on Scientific Computing* **2008**, *30* (6), 3126–3149. https://doi.org/10.1137/070692017.

(65) Radhakrishnan, K.; Halász, Á.; McCabe, M. M.; Edwards, J. S.; Wilson, B. S. Mathematical Simulation of Membrane Protein Clustering for Efficient Signal Transduction. *Ann Biomed Eng* **2012**, *40* (11), 2307–2318. https://doi.org/10.1007/s10439-012-0599-z.

(66) Avdagić, N.; Zaćiragić, A.; Babić, N.; Hukić, M.; Šeremet, M.; Lepara, O.; Nakaš-Ićindić, E. Nitric Oxide as a Potential Biomarker in Inflammatory Bowel Disease. *Bosn J Basic Med Sci* **2013**, *13* (1), 5. https://doi.org/10.17305/bjbms.2013.2402.

(67) Lacruz-Guzmán, D.; Torres-Moreno, D.; Pedrero, F.; Romero-Cara, P.; García-Tercero, I.; Trujillo-Santos, J.; Conesa-Zamora, P. Influence of Polymorphisms and TNF and IL1β Serum Concentration on the Infliximab Response in Crohn's Disease and Ulcerative Colitis. *Eur J Clin Pharmacol* **2013**, *69* (3), 431–438. https://doi.org/10.1007/s00228-012-1389-0.

(68) Iwaki, T.; Hara, K.; Umemura, K. Nanobody Production Can Be Simplified by Direct Secretion from Escherichia Coli. *Protein Expr Purif* **2020**, *170*, 105607. https://doi.org/10.1016/j.pep.2020.105607.

(69) Sender, R.; Fuchs, S.; Milo, R. Revised Estimates for the Number of Human and Bacteria Cells in the Body. *PLoS Biol* **2016**, *14* (8), e1002533. https://doi.org/10.1371/journal.pbio.1002533.

(70) McCallum, G.; Tropini, C. The Gut Microbiota and Its Biogeography. *Nat Rev Microbiol* **2023**. https://doi.org/10.1038/s41579-023-00969-0.

(71) Stein, R. R.; Tanoue, T.; Szabady, R. L.; Bhattarai, S. K.; Olle, B.; Norman, J. M.; Suda, W.; Oshima, K.; Hattori, M.; Gerber, G. K.; Sander, C.; Honda, K.; Bucci, V. Computer-Guided Design of Optimal Microbial Consortia for Immune System Modulation. *Elife* **2018**, *7*. https://doi.org/10.7554/eLife.30916.

(72) Aogo, R. A.; Tanaka, M. M.; Penington, C. J. Spatial Dynamics of Inflammation-Causing and Commensal Bacteria in the Gastrointestinal Tract. *J Theor Biol* **2022**, *548*, 111194. https://doi.org/10.1016/j.jtbi.2022.111194.

(73) Labarthe, S.; Polizzi, B.; Phan, T.; Goudon, T.; Ribot, M.; Laroche, B. A Mathematical Model to Investigate the Key Drivers of the Biogeography of the Colon Microbiota. *J Theor Biol* **2019**, *462*, 552–581. https://doi.org/10.1016/j.jtbi.2018.12.009.

(74) Arciero, J. C.; Ermentrout, G. B.; Upperman, J. S.; Vodovotz, Y.; Rubin, J. E. Using a Mathematical Model to Analyze the Role of Probiotics and Inflammation in Necrotizing Enterocolitis. *PLoS One* **2010**, *5* (4), e10066. https://doi.org/10.1371/journal.pone.0010066.

(75) Maria Spagnuolo, A.; DiRita, V.; Kirschner, D. A Model for Vibrio Cholerae Colonization of the Human Intestine. *J Theor Biol* **2011**, *289*, 247–258. https://doi.org/10.1016/j.jtbi.2011.08.028.

(76) Thomas, D. D.; Liu, X.; Kantrow, S. P.; Lancaster, J. R. The Biological Lifetime of Nitric Oxide: Implications for the Perivascular Dynamics of NO and O_2. *Proceedings of the National Academy of Sciences* **2001**, *98* (1), 355–360. https://doi.org/10.1073/pnas.98.1.355.

(77) Malinski, T.; Taha, Z.; Grunfeld, S.; Patton, S.; Kapturczak, M.; Tomboulian, P. Diffusion of Nitric Oxide in the Aorta Wall Monitored in Situ by Porphyrinic Microsensors.

Biochem Biophys Res Commun **1993**, *193* (3), 1076–1082. https://doi.org/10.1006/bbrc.1993.1735.

(78) Triassi, A. J.; Fields, B. D.; Monahan, C. E.; Means, J. M.; Park, Y.; Doosthosseini, H.; Padmakumar, J. P.; Isabella, V. M.; Voigt, C. A. Redesign of an Escherichia Coli Nissle Treatment for Phenylketonuria Using Insulated Genomic Landing Pads and Genetic Circuits to Reduce Burden. *Cell Syst* **2023**, *14* (6), 512-524.e12. https://doi.org/10.1016/j.cels.2023.05.004.

(79) Wu, G.; Yan, Q.; Jones, J. A.; Tang, Y. J.; Fong, S. S.; Koffas, M. A. G. Metabolic Burden: Cornerstones in Synthetic Biology and Metabolic Engineering Applications. *Trends Biotechnol* **2016**, *34* (8), 652–664. https://doi.org/10.1016/J.TIBTECH.2016.02.010.

(80) Borkowski, O.; Ceroni, F.; Stan, G. B.; Ellis, T. Overloaded and Stressed: Whole-Cell Considerations for Bacterial Synthetic Biology. *Curr Opin Microbiol* **2016**, *33*, 123–130. https://doi.org/10.1016/J.MIB.2016.07.009.

(81) Elowitz, M. B.; Levine, A. J.; Siggia, E. D.; Swain, P. S. Stochastic Gene Expression in a Single Cell. *Science (1979)* **2007**, *297* (2002), 1183–1186. https://doi.org/10.1126/science.1070919.

(82) Bandiera, L.; Furini, S.; Giordano, E. Phenotypic Variability in Synthetic Biology Applications: Dealing with Noise in Microbial Gene Expression. *Frontiers in Microbiology*. 2016. https://doi.org/10.3389/fmicb.2016.00479.

(83) Tropini, C.; Earle, K. A.; Huang, K. C.; Sonnenburg, J. L. The Gut Microbiome: Connecting Spatial Organization to Function. *Cell Host Microbe* **2017**, *21* (4), 433–442. https://doi.org/10.1016/J.CHOM.2017.03.010.

(84) Del Vecchio, D.; Qian, Y.; Murray, R. M.; Sontag, E. D. Future Systems and Control Research in Synthetic Biology. *Annu Rev Control* **2018**, *45*, 5–17. https://doi.org/10.1016/J.ARCONTROL.2018.04.007.

(85) Choudhary, R.; Mahadevan, R. Toward a Systematic Design of Smart Probiotics. *Curr Opin Biotechnol* **2020**, *64*, 199–209. https://doi.org/10.1016/J.COPBIO.2020.05.003.

(86) Rohlhill, J.; Sandoval, N. R.; Papoutsakis, E. T. Sort-Seq Approach to Engineering a Formaldehyde-Inducible Promoter for Dynamically Regulated Escherichia Coli Growth on Methanol. *ACS Synth Biol* **2017**, *6* (8), 1584–1595. https://doi.org/10.1021/ACSSYNBIO.7B00114/SUPPL_FILE/SB7B00114_LIVESLIDES.MP4.

(87) Cobb, R. E.; Sun, N.; Zhao, H. Directed Evolution as a Powerful Synthetic Biology Tool. *Methods* **2013**, *60* (1), 81–90. https://doi.org/10.1016/j.ymeth.2012.03.009.

(88) Westmann, C. A.; Guazzaroni, M.-E.; Silva-Rocha, R. Engineering Complexity in Bacterial Regulatory Circuits for Biotechnological Applications. *mSystems* **2018**, *3* (2), e00151-17. https://doi.org/10.1128/mSystems.00151-17.

(89) Westmann, C. A.; Goldbach, L.; Wagner, A. The Highly Rugged yet Navigable Regulatory Landscape of the Bacterial Transcription Factor TetR. *bioRxiv* **2023**, 2023.08.25.554764. https://doi.org/10.1101/2023.08.25.554764.

(90) Moon, T. S. Probiotic and Microbiota Engineering for Practical Applications. *Curr Opin Food Sci* **2024**, *56*, 101130. https://doi.org/10.1016/J.COFS.2024.101130.

(91) Barra, M.; Danino, T.; Garrido, D. Engineered Probiotics for Detection and Treatment of Inflammatory Intestinal Diseases. *Front Bioeng Biotechnol* **2020**, *8*, 521594. https://doi.org/10.3389/FBIOE.2020.00265/BIBTEX.

(92) Brooks, S. M.; Alper, H. S. Applications, Challenges, and Needs for Employing Synthetic Biology beyond the Lab. *Nature Communications 2021 12:1* **2021**, *12* (1), 1–16. https://doi.org/10.1038/s41467-021-21740-0.

(93) Kumar, S.; Hasty, J. Stability, Robustness, and Containment: Preparing Synthetic Biology for Real-World Deployment. *Curr Opin Biotechnol* **2023**, *79*, 102880. https://doi.org/10.1016/j.copbio.2022.102880.

(94) Ingram, D.; Stan, G. B. Modelling Genetic Stability in Engineered Cell Populations. *Nature Communications 2023 14:1* **2023**, *14* (1), 1–12. https://doi.org/10.1038/s41467-023-38850-6.

(95) Olier, M.; Marcq, I.; Salvador-Cartier, C.; Secher, T.; Dobrindt, U.; Boury, M.; Bacquié, V.; Penary, M.; Gaultier, E.; Nougayrède, J. P.; Fioramonti, J.; Oswald, E. Genotoxicity of Escherichia Coli Nissle 1917 Strain Cannot Be Dissociated from Its Probiotic Activity. *Gut Microbes* **2012**, *3* (6), 501. https://doi.org/10.4161/GMIC.21737.

(96) Nougayrède, J.-P.; Chagneau, C. V.; Motta, J.-P.; Bossuet-Greif, N.; Belloy, M.; Taieb, F.; Gratadoux, J.-J.; Thomas, M.; Langella, P.; Oswald, E. A Toxic Friend: Genotoxic and Mutagenic Activity of the Probiotic Strain Escherichia Coli Nissle 1917. *mSphere* **2021**, *6* (4). https://doi.org/10.1128/MSPHERE.00624-21.

(97) Tramontano, M.; Andrejev, S.; Pruteanu, M.; Klünemann, M.; Kuhn, M.; Galardini, M.; Jouhten, P.; Zelezniak, A.; Zeller, G.; Bork, P.; Typas, A.; Patil, K. R. Nutritional Preferences of Human Gut Bacteria Reveal Their Metabolic Idiosyncrasies. *Nature Microbiology 2018 3:4* **2018**, *3* (4), 514–522. https://doi.org/10.1038/s41564-018-0123-9.

(98) A Heinken, G. A. D. R. J. H. M. N. O. O. AGORA2: Large Scale Reconstruction of the Microbiome Highlights Wide-Spread Drug-Metabolising Capacities. *bioRxiv* **2020**. https://doi.org/10.1101/2020.11.09.375451.

(99) van 't Hof, M.; Mohite, O. S.; Monk, J. M.; Weber, T.; Palsson, B. O.; Sommer, M. O. A. High-Quality Genome-Scale Metabolic Network Reconstruction of Probiotic Bacterium Escherichia Coli Nissle 1917. *BMC Bioinformatics* **2022**, *23* (1), 1–23. https://doi.org/10.1186/S12859-022-05108-9/FIGURES/4.

(100) Nørholm, M. H. H. Meta Synthetic Biology: Controlling the Evolution of Engineered Living Systems. *Microb Biotechnol* **2018**, 1751-7915.13350. https://doi.org/10.1111/1751-7915.13350.

(101) Mays, Z. J. S.; Chappell, T. C.; Nair, N. U. Quantifying and Engineering Mucus Adhesion of Probiotics. *ACS Synth Biol* **2020**, *9* (2), 356–367. https://doi.org/10.1021/acssynbio.9b00356.

(102) Kan, A.; Gelfat, I.; Emani, S.; Praveschotinunt, P.; Joshi, N. S. Plasmid Vectors for *in Vivo* Selection-Free Use with the Probiotic *E. Coli* Nissle 1917. *ACS Synth Biol* **2021**, *10* (1), 94–106. https://doi.org/10.1021/acssynbio.0c00466.

(103) Sundaram, L. S.; Ajioka, J. W.; Molloy, J. C. Synthetic Biology Regulation in Europe: Containment, Release and Beyond. *Synth Biol* **2023**, *8* (1). https://doi.org/10.1093/synbio/ysad009.

(104) Donati, S.; Barbier, I.; García-Soriano, D. A.; Grasso, S.; Handal-Marquez, P.; Malcı, K.; Marlow, L.; Westmann, C.; Amara, A. Synthetic Biology in Europe: Current Community Landscape and Future Perspectives. *Biotechnology Notes* **2022**, *3*, 54–61. https://doi.org/10.1016/J.BIOTNO.2022.07.003.

(105) Karabin, J.; Mansfield, I.; Frow, E. K. Exploring Presentations of Sustainability by US Synthetic Biology Companies. *PLoS One* **2021**, *16* (9), e0257327. https://doi.org/10.1371/JOURNAL.PONE.0257327.

(106) Voigt, C. A. Synthetic Biology 2020–2030: Six Commercially-Available Products That Are Changing Our World. *Nat Commun* **2020**, *11* (1), 6379. https://doi.org/10.1038/s41467-020-20122-2.